Testing the theory of radiation belt electron loss by hiss and electromagnetic ion cyclotron waves

Ling Zheng

A dissertation
submitted in partial fulfillment of the
requirements for the degree of

Doctor of Philosophy

University of Washington

2019

Reading Committee:

Michael P. McCarthy, Chair

Robert Holzworth

Robert Winglee

Program Authorized to Offer Degree:
Earth and Space Sciences

University of Washington

Abstract

Testing the theory of radiation belt electron loss by hiss and electromagnetic ion cyclotron waves

Ling Zheng

Chair of the Supervisory Committee:
Professor Michael P. McCarthy
Department of Earth and Space Sciences

Hiss, chorus and electromagnetic ion cyclotron waves (EMIC wave) are three major wave modes that are widely investigated and included in the radiation belt electron models to explain electron precipitation. The quasi-linear theories of electron loss through pitch angle diffusion by hiss and EMIC waves were proposed in 1970s. Since then the testing of the theories is still going on though some progresses had been made. Comparison of theoretical predictions to electrons distribution at loss cone is one effective way to evaluate the theories. The main obstruction of loss cone testing was from the lack of measurements of the electron loss cone distribution with enough pitch angle and energy resolution and simultaneous wave activities at the heart of radiation belt. This thesis is devoted to testing the hiss and EMIC waves diffusion theories from the perspective of the electron loss cone distribution by utilizing the previously unnoticed overlap of UARS and CRRES missions in 1991. The conclusions are as following: (1) Two cases showing the consistency between quasi-linear theory of hiss diffusion and observed loss cone distribution are found. (2) In 25 out of 38 cases, hiss wave power is far insufficient in precipitating the large amount of electrons observed. Loss mechanisms other than hiss, chorus and EMIC waves are needed to account for the discrepancy. (3) Three EMIC wave events were investigated. In the first case, the isotropic distribution (sign of strong diffusion) is caused by process other than EMIC wave

diffusion demonstrating that simultaneous presence of EMIC wave and electron precipitation does not guarantee any connection between the two. Large discrepancy between quasi-linear theory of EMIC wave diffusion and observed electron loss cone distribution is found from the second case. The strong depletion of electrons by EMIC waves predicted by the current theory was not found. In the third case the resonant energy goes beyond the instrument limit of electron detectors thus no conclusion is drawn.

TABLE OF CONTENTS

Page

List of Figures iii

Chapter 1: Introduction 1
1.1 Radiation belt and relativistic electrons 1
1.2 Previous research on hiss wave as a loss mechanism 3
1.3 Previous research on electromagnetic ion cyclotron wave as a loss mechanism 6
1.4 Motivation, science question and outline of this thesis 10

Chapter 2: Data set 13
2.1 UARS satellite 13
2.2 CRRES satellite 15
2.3 UARS and CRRES magnetic conjunction 17

Chapter 3: Theoretic framework of quasi-linear diffusion 21
3.1 Wave-particle interaction as a diffusion process 21
3.2 Formula of pitch angle diffusion coefficient 25

Chapter 4: Comparison of hiss wave diffusion theory to electron loss cone distribution 31
4.1 Electron precipitation events consistent with hiss diffusion 33
4.2 Electron precipitation events inconsistent with hiss diffusion 36
4.3 Conclusion for hiss diffusion theory testing 41

Chapter 5: Comparison of EMIC wave diffusion to precipitating and trapped electrons both at low Earth orbit and magnetic equator 42
5.1 Case studies 42
5.2 Concluding remarks from case studies 56
5.3 Comparison to findings from others 56
5.4 Conclusions of testing EMIC wave diffusion theory 60

Chapter 6: Conclusion and future work 61

Bibliography 62

Appendix A: 68
A.1 Derivation of $N(\omega)$ for hiss diffusion coefficient 68
A.2 Derivation of $N(Y)$ for EMIC diffusion coefficient 69
A.3 Source term estimation using observations inside loss cone 69
A.4 Some notes on diffusion coefficients code implementation and testing 70

LIST OF FIGURES

Figure Number Page

1.1 schematic view of Earth's magnetosphere formed by interaction of Earth's magnetic field and solar wind. The ball at the center is Earth with arrow curves the magnetic field lines. The green shaded area are inner and outer radiation belts. Credit from spaceweathercenter.org 2

2.1 Orientation of UARS HEPS electron telescopes 14

2.2 schematic view of a magnetic conjunction between UARS at 585km and CRRES at about 33,000km magnetic equator. 18

2.3 Temporal distribution of 38 conjunction cases in Oct 1991. 19

2.4 Spatial distribution of 38 conjunction cases in Oct 1991. 20

4.1 Survey plot of wave power spectrum from CRRES PWE (Plasma Wave Experiment) on Oct 8th, 1991, Orbit 1059. The plot is provided by Physics Department , University of Iowa. Th broad band hiss is typically from tens of Hz to 2 kHz. The red line is electron cyclotron frequency. 32

4.2 Hiss wave power spectra at 21:15:00-21:15:54, Oct 8, 1991 when UARS and CRRES are at magnetic conjunction 34

4.3 Comparison of hiss diffusion curve to measured electron flux at loss cone. he vertical magenta dash line plots edge of bounce loss cone. **(a)** 100 keV electron flux vs hiss diffusion, the red stars are measured electron flux from three electron telescopes inside loss cone , the horizontal color bars are field of view of each telescope, the thick blue curve is electron flux distribution predicted by hiss diffusion, the black stars are integral of blue curve over field of view of each telescope, the dash blue curve is obtained by reducing source term by a factor of 2. **(b)** similar to panel (a) for 500 keV electrons. **(c)** similar to panel (a), for 1MeV electrons 35

4.4 Comparison of modified hiss diffusion curve to measured electron flux at loss cone. The vertical magenta dash line plots edge of bounce loss cone whereas the horizontal green dash line is detector sensitivity.**(a)** 100 keV electron flux vs hiss diffusion, the red stars are measured electron flux from three electron telescopes inside loss cone , the horizontal color bars are field of view of each telescope, the thick blue curve is electron flux distribution predicted by hiss diffusion with diffusion coefficient increased by a factor of 10,000, the black stars are integral of blue curve over field of view of each telescope. **(b)** similar to panel (a) for 500 keV electrons with diffusion coefficient boosted up by a factor of 2000. **(c)** similar to panel (a), for 1MeV electrons with diffusion coefficient boosted up by a factor of 2000 37

4.5 Comparison of hiss diffusion curve to measured electron flux at loss cone. The vertical magenta dash line plots edge of bounce loss cone. **(a)** 100 keV electron flux vs hiss diffusion, the red stars are measured electron flux from three electron telescopes inside loss cone , the horizontal color bars are field of view of each telescope, the thick blue curve is electron flux distribution predicted by hiss diffusion. **(b)** similar to panel (a) for 500 keV electrons **(c)** similar to panel (a), for 1MeV electrons 38

4.6 Electron flux pitch angle profile with sharp edge of loss cone and flat distribution inside loss cone. The vertical magenta dash line plots edge of bounce loss cone. The horizontal green dash line is detector sensitivity 39

4.7 Comparison of hiss diffusion curve to measured electron flux at loss cone. The the vertical magenta dash line plots edge of bounce loss cone. The horizontal green dash line is detector sensitivity. **(a)** 100 keV electron flux vs hiss diffusion, the red stars are measured electron flux from three electron telescopes inside loss cone , the horizontal color bars are field of view of each telescope, the thick blue curve is electron flux distribution predicted by hiss diffusion, the dash blue line is hiss curve with diffusion coefficient decreased by a factor of 10, **(b)** similar to panel (a) for 500 keV electrons **(c)** similar to panel (a), for 1MeV electrons 40

5.1 Three EMIC wave events from CRRES with case 1 on October 1st, 1991 and case 2 and 3 at two consecutive orbits on Oct 4th, 1991. The right column panels plot wave power spectrum on frequency domain versus universal time, L shell and magnetic local time. The black double lines on UT axis marks the time slots when UARS is at footprint of CRRES (aka conjunction). The red double line marks the reference time. Two white dash lines from top to bottom within each panel are local hydrogen and helium gyro-frequencies. The left column panels plot wave power spectrum at the time slots marked the double black and red lines in the right column. The black curve is wave power spectrum at the conjunction time while red curve is wave power at reference time. The blue vertical dash lines show cutoff frequencies bounding the peaks. 43

5.2 Trapped and precipitating electron flux observed by UARS at three UARS/CRRES conjunctions. The left,middle and right columns correspond to case 1,2, and 3 respectively. From top to bottom, **(a)** 0.5 MeV electron differential flux with red for electron telescope right outside loss cone , blue, green and cyan for three telescopes well inside loss cone, the horizontal magenta dash lines show detector sensitivity, those below sensitivity line are due to over-correction of correction algorithm, **(b)** and **(c)**1MeV and 2MeV electron differential flux with color code the same as 0.5 MeV electrons. The events pointed by the two black arrows are re-plotted in Figure 5.3 and 5.4. **(d)** difference of L shell and magnetic local time of UARS (magenta) and CRRES(blue),**(e)** L profile of 1MeV electron flux at time window of one minute right before and after conjunction, red for electron telescope right outside loss cone, blue, green and cyan for three telescopes well inside loss cone. The vertical two black dash lines bound the conjunction window. 45

5.3 Comparison of theoretical loss cone distribution to measurements from UARS around 21:55 UT, Oct 4, 1991. The diffusion coefficients are computed assuming parallel propagating EMIC waves. Row (a) and (b) are for 2MeV and 1MeV electrons respectively. The red thick curves are prediction given by EMIC wave diffusion theory. Red dash lines are EMIC wave curve with diffusion coefficients decreased by a factor of 16 for 1MeV electrons and 13 for 2 MeV electrons. The black dots are electron differential flux measured by four telescopes on board UARS with one right outside loss cone, three inside loss cone. The horizontal error bars are field of view of telescopes. The pink vertical dash lines mark the edge of bounce loss cone. The detector sensitivity is marked by horizontal blue dash lines. The pitch angles of UARS telescopes at low Earth orbit are converted into equatorial values in degree. 49

5.4 Similar to Figure 5.3, assuming oblique propagating EMIC waves 50

5.5 Precipitating protons from UARS at 550km. The upper and bottom panels plot proton flux at pitch angle 22° and 14° respectively. Both are well inside bounce loss cone. The UARS /CRRES conjunction is at 20:54:30 to 20:55:20 well inside the proton precipitation window. The lower energy cutoff is 74 keV. Notice that the energy is in eV and flux is in $cm^{-2}s^{-1}sr^{-1}eV^{-1}$. 51

5.6 Two choices of cutoff frequencies. The black curve is wave power spectrum at case 2 conjunction around 21:55 UT, Oct 4, 1991. The green curve is the wave power spectrum used as background and measured around 20:21 UT, Oct 4, 1991. The magenta vertical dash line marks lower end cutoff frequency of 0.45 Hz, blue and red lines mark two choices of cutoff frequencies of 1.665 Hz and 2.1 Hz at higher end 52

5.7 Comparison of trapped electron from MEA on board CRRES to EMIC wave diffusion. **(a)** differential flux of 1090 keV electrons at pitch angles from 5° to 90°. **(b)** thick blue curve is 1090 keV electron differential flux at pitch angle of 5° measured by MEA. The thin solid red line is prediction from EMIC wave diffusion with bounce-drift averaged model. The dash magenta line is prediction from EMIC wave diffusion with bounce-averaged model. **(c)**EMIC wave spectrogram versus universal time, L shell and magnetic local time. The two white meandering dash lines from top to bottom mark local hydrogen and helium gyro-frequencies. 53

5.8 hydrogen band EMIC wave amplitude square versus electron flux at pitch angle of 5° measured by MEA on board CRRES. The black and red dots are for 509 keV and 1090 keV respectively. 55

5.9 snapshot of Figure 3 of Miyoshi et al 2008 [38].(a) Emission profile of Hb and (be) count rates of energetic ions and electrons observed by POES-17 on September 5, 2005 with UT, MLAT, the McIlwain L-value, and magnetic local time (MLT) of the satellite footprint during the period when the satellite was crossing over Athabasca. The vertical blue line indicates the time when the satellite footprint crossed the stable isolated proton aurora. MLAT and L-value are calculated by the IGRF model. 58

5.10 Snapshot of Figure 8 of Zhang XJ et al 2016 [56].(a) Observed electron pitch angle distributions from Van Allen Probes at L = 5.77. (b) The evolution of electron distribution after interaction with EMIC and hiss, (c) only EMIC, and (d) only hiss waves for 40 min. Initial distributions are shown in dotted lines; observations or model results at t = 40 min are shown in solid lines. . . 59

ACKNOWLEDGMENTS

I appreciate UW Department of Earth and Space Sciences and my advisor Prof. Michael P. McCarthy for supporting me with RA, TA and fellowships through my entire life pursuing this doctorate degree of space physics. I also thank Michael for great support and close advising for so many years and Profs. Robert Holzworth, Robert Winglee and Erika Harnett for being in my committee to make sure that I am on the right track. I thank Profs. Michael McCarthy, Robert Holzworth and Robert Winglee sitting in my reading committee to prove this thesis. Thanks Prof. Robert Holzworth for admitting me to this department. I thank Rudy Frahm , Pesnell William, Gaines Edward from UARS PEM group for help with electron data and IDL code for loading the data. Rudy Frahm provided details about correction algorithm which is useful for interpretation of electron spectrum. I would also like to thank Larry Granroth from University of Iowa for offering the CRRES plasma wave CDF files generated by French Aerospace Lab (ONERA). The wave plots from website hosted by Physics department of University of Iowa were used along with ONERA cdf files. Since CRRES plasma wave data was not publicly archived, this work is not possible without the help of people from University of Iowa. Dr Nigel Meredith from British Antartic Survey kindly provided me raw EMIC wave data and good feedback on data analysis. The EMIC wave investigation would not be possible without Dr Meredith's help. I thank emeritus Professor Brian Fraser from University of Newcastle for providing the detailed list and plots of EMIC wave events. The communication with my friend Yong Fu Wang from School of Earth and Space Science, Peking University is helpful to better understand the quasi-linear theory of plasma wave diffusion and navigating through MATLAB code. The discussion with office mates Hao Zheng, Paul Sturmer and Todd Anderson were also beneficial.

DEDICATION

to the readers

Chapter 1

INTRODUCTION

This chapter will start with the basics of radiation belt, the source and loss processes that control the flux of relativistic electrons inside the outer part of radiation belt. Hiss and electromagnetic ion cyclotron waves (EMIC wave) were proposed in 1970s to be two important electromagnetic waves in radiation belt that precipitate radiation belt electrons into Earth's atmosphere via a process named pitch angle diffusion. A review on quasi-linear theories of hiss and EMIC waves diffusion as well as a summary of observations will be presented in details. This chapter will conclude with the motivation, science questions and the outline of following chapters.

1.1 Radiation belt and relativistic electrons

The Earth's magnetic field is produced by the liquid at core and its effects extend to outer space. It interacts with the continuous flow of magnetized charged particles from the Sun named solar wind forming Earth's magnetosphere which is the outermost boundary of Earth's territory. The magnetosphere is compressed in the day side and stretched at nightside (See Figure1.1). Within magnetosphere, the radiation belt is located about 1.1 to 8 Earth radii from center of the Earth. It is also called Van Allen belt after Dr James Van Allen who discovered it in 1958[53]. Radiation belt is further divided into two parts by the slot region of very few energetic electrons at 2 to 3 Earth radii. The inner belt is relatively stable. Outer radiation belt is very dynamic and is famous for relativistic electrons that are a threat to the nearby satellites. The energy of relativistic electrons concerned here is above 100,000 electron volts (100 keV).

The flux of outer radiation belt electrons is highly dynamic and can fluctuate several

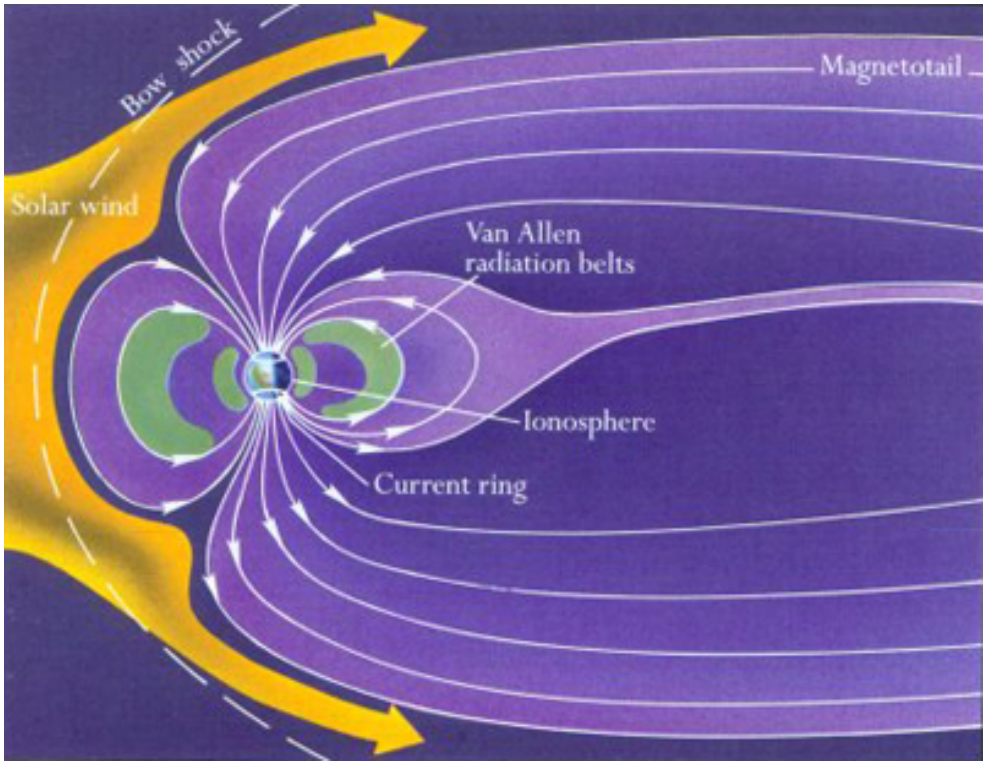

Figure 1.1: schematic view of Earth's magnetosphere formed by interaction of Earth's magnetic field and solar wind. The ball at the center is Earth with arrow curves the magnetic field lines. The green shaded area are inner and outer radiation belts. Credit from spaceweathercenter.org

orders of magnitude in time scales of days, hours and even shorter. The local electron flux is determined by the relative strength of source and loss. Solar wind and Earth's atmosphere provide seed electrons which can be further energized by a variety of processes. As electrons are transported radially toward the Earth through Earth's approximately dipole magnetic field, and energized through adiabatic processes. The energetic electrons can also be built up locally by very low frequency and ultra low frequency waves. When the solar wind is very strong and push the dayside boundary of magnetosphere into geosynchronous orbit, radiation belt electrons are lost to interplanetary space by crossing the magnetopause. Radiation

belt electrons are also being precipitated into Earth's north and south polar atmosphere by ELF/VLF electromagnetic or electrostatic waves via a process called pitch angle diffusion. The electron precipitation can be detected by satellites at low Earth orbit of several hundred kilometers above the Earth's surface. The bremsstrahlung X-rays associated with precipitating electrons can be detected by stratospheric balloon experiments.

ELF/VLF(from 20 Hz to 30 kHz) electromagnetic waves, of both natural and anthropogenic origins, were proposed as mechanisms that dump radiation belt electrons into Earth's atmosphere via pitch angle diffusion not long after the discovery of radiation belt. Pitch angle is the angle between electron velocity and local Earth's magnetic field. At the magnetic equator electrons with near zero or 180 degree pitch angle can move along the magnetic field line freely traveling from radiation belt toward the thick atmosphere and get lost. Electrons with equatorial pitch angle close to 90 degree are trapped in Earth's magnetic field. The small range of pitch angle near either zero or 180 degree forms a region called loss cone. The electrons within loss cone will get lost quickly whereas those outside loss cone will stay trapped. The Lorentz force of the waves either accelerate or decelerate the electrons, increase or decrease the pitch angle of electrons randomly. Depending on the distribution function of electrons and properties of the waves, the pitch angle and energy diffusion will go in certain direction. If the trapped electron flux is larger than flux of electrons inside loss cone which is always true in outer radiation belt, the waves will move electrons from large pitch angle to small pitch angle to smooth out the gradient. Some very low frequency electron cyclotron waves [24]and ultra low frequency ion cyclotron waves(e.g. EMIC waves) are able to reduce the pitch angle of trapped electrons and thus precipitate them into Earth's atmosphere.

1.2 Previous research on hiss wave as a loss mechanism

1.2.1 Basics of hiss wave and the theory of hiss as a loss mechanism

Hiss wave is broad band incoherent electron cyclotron waves that is observed mostly inside plasmasphere which largely overlaps with radiation belt in space and is filled with dense cold

electrons of several electron volt during both geomagnetically active and quiet time. The frequency of hiss can go up to 2 kHz and reach to as low as 20 Hz, with most wave power at several hundred Hz[32]. Hiss was first proposed by Lyons et al in 1970s [32, 31] as the main mechanism inside plasmasphere that precipitate electrons via pure pitch angle diffusion forming the slot region that separates the inner and outer radiation belt. More details about the theoretic framework of hiss diffusion is in Chapter 3.

1.2.2 Evidence hunting

The hiss diffusion theory has been backed by general agreement with profile of trapped electrons. Relying on simple models of hiss wave and cold plasma density, Lyons [32] computed pitch angle profile and decay rate of trapped electrons. Agreement with observations from Ogo-5 and OV3-3 satellites was found in slot regions. The hiss was assumed by Lyons to be uniform over entire plasmasphere. Utilizing electrons and hiss waves measured by CRRES spacecraft, Meredith in 2006 reported the decay time of trapped electrons at pitch angle of 90° to be consistent with pitch angle scattering by hiss traveling at small and moderate wave normal angles (the angle between local Earth's magnetic field and wave vector)[35] . Similarly to Lyons' work [32], this comparison is on average and over long term (days, weeks or months) though a more realistic global model of hiss was adopted. More recently Thorne in 2013 [48] reported that the slow decay of an unusual new ring of relativistic electrons in outer radiation belt can be well explained by global plasmaspheric hiss scattering.

The comparison of hiss wave to trapped electrons has limitations. The hiss diffusion is weak most of the time due to its small amplitude of several picotesla. The trapped electron flux is several orders of magnitude of higher than precipitating flux. A small bite on trapped electrons by hiss could be not noticeable. Back to early 1990s, Imhof [18] found that time variation of electron flux inside loss cone resembles the variation of hiss wave amplitude while electron flux just outside loss cone doesn't correlate with hiss wave variation at all. This is similar to a recent discovery by Kasahara in early 2018 about interaction of electrons with chorus wave which like hiss is also whistler mode electron cyclotron wave and considered as

important mechanism for electron precipitation [23]. Kasahara concluded that chorus waves strongly modulate electron flux inside loss cone while showing no clear effect on electrons outside loss cone. In order to see the effects of hiss scattering, a long time observation is needed. At longer time frame the hiss scattering is easier to be obscured by other processes. An incomplete list of processes of concerned includes radial diffusion, local acceleration, electron loss through magnetosphere boundary crossing, ring current effect, and wave modes other than hiss.

The electrons inside the loss cone are very sensitive to wave scattering which makes one-to-one correspondence testing possible. Testing the hiss theory with electrons inside loss cone also eliminates possibilities of loss processes other than precipitation. Some attempt had been made on this since not long after Lyons [32] suggested hiss as loss mechanism responsible for radiation belt electron precipitation. In early 1980s Imhof et al [16] investigated 17 conjunctions between P78-1 at 600km and ISEE-1 at 2 to 3 earth radii in the magnetosphere. Hiss wave measurements from ISEE-1, along with cold plasma density inferred from upper hybrid frequency, were compared to simultaneous measurements of quasi-trapped($65^\circ - 115^\circ$ pitch angle at low Earth orbit) electron spectra (68 -1120 keV) at P78-1. In general the wave frequency, electron energy and cold plasma density were found mutually consistent with precipitation caused by first order cyclotron resonance with parallel propagating hiss at the equator. As mentioned earlier Imhof et al in early 1990s [18] reported good correlation between loss cone electron flux and hiss wave observed by CRRES spacecraft at the vicinity of magnetic equator. The best correlation between waves and electrons is seen for wave near 256Hz and electrons near 50keV. Li et al in 2014 [26] compared the ratio of integral electron flux between two electron telescopes (approximately 0° and 90°pitch angles) on board POES satellite to that predicted by hiss diffusion under steady state assumption when POES is at magnetic footprint of Van Allen probes. The POES measurement agrees with estimation from hiss diffusion within a factor of 10. Breneman et al in 2015 [8] investigated two cases when hiss waves were observed by Van Allen probes and simultaneously measurements of X-rays associated with precipitating electrons were seen by high altitude balloon

arrays(BARREL) at the magnetic footprint. The temporal structure of X-rays resembles hiss variation. Hardman et al in 2015 [15] used ground-based VLF receiver network to investigate electron precipitation during a magnetic storm. The weak electron precipitation that's missed by POES but captured by their network is claimed to be consistent with hiss diffusion.

In summary, the long term averaged trapped electrons profile is found to be consistent with hiss diffusion theory. Some attempt of looking into loss cone had been made.

1.3 Previous research on electromagnetic ion cyclotron wave as a loss mechanism

1.3.1 Basics of EMIC wave and the theory of EMIC wave as a loss mechanism

Electromagnetic Ion Cyclotron Wave (EMIC) is at Pc1 and 2 bands of ultra lower frequency with a typical frequency range of 0.1-5Hz. EMIC wave consists of three distinct bands: hydrogen band with frequency lower than proton gyro-frequency and above He+ gyro-frequency, helium band with frequency in between He+ gyro-frequency and O+ gyro-frequency and oxygen band which is below O+ gyro-frequency but higher than Alfvenic ULF waves at Pc3- Pc5. EMIC waves arise when ion temperature perpendicular to local magnetic field is larger than parallel temperature. The temperature anisotropy is caused by substorm injections, ring current intensification during magnetic storms and solar wind impulse in dayside magnetosphere.

Thorne and Kennel in 1971 [47] first introduced EMIC waves as loss mechanism for precipitating relativistic electrons into atmosphere. One year later Lyons and Thorne further addressed the EMIC wave theory with more quantitative framework [30]. The features of electron precipitation associated with EMIC waves are summarized as following. First, EMIC waves are generated by temperature anisotropy of tens of keV ring current ions with the perpendicular temperature much higher than parallel temperature. Thus it is often to see that relativistic electron precipitation is accompanied by almost simultaneous ion precipitation. Second, due to the large amplitude of EMIC waves with typical value of

1-10nT, the pitch angle diffusion could reach strong diffusion limit such that an isotropic distribution of electrons across loss cone is expected. Also due to strong diffusion, the trapped electron flux will decrease in a fast pace at the absence of a strong source to replenish the electrons. Summers calculations in 2003 suggested that during magnetic storms EMIC waves can remove the electrons completely in several hours even though waves reside at only one percent of magnetic local time [46].Third, the minimum resonant energy of electrons is 1MeV suggested by Thorne and Kennel in 1971 due to the ultra low frequency nature of EMIC waves. Electrons with energy lower than 1 MeV was believed to not interact with EMIC waves. Later theories show the minimum resonant energy can go down to several hundred keV[36] and even at 100 keV under nonlinear resonance[39]. Fourth, EMIC waves can only scatter electrons at small to medium pitch angles leaving electrons around 90° intact, due to zero overlap between cyclotron resonance and Landau resonance for relativistic electrons. Last, Thorne and Kennel predicted that relativistic electrons precipitation (REPs) will be mostly in the dusk sector from evening to midnight in magnetic local time and confined in L = 3.5-5 at the vicinity of plasmapause. This is straightforward inference from ring current ion drifting path and high cold plasma density of plasmasphere. The cloud of ring current ions injected from midnight plasmasheet drift westward into dusk side and then go to morning side. The high cold plasma density inside plasmasphere greatly lowers the resonant energy from tens of MeV to several hundred keV.

1.3.2 Evidence hunting

Strong electron precipitation accompanied by simultaneous proton precipitation is believed to be an important though not unique signature of EMIC wave scattering. Thorne and Andreoli in 1980 [49] investigated 313 relativistic electron precipitation(REP) events from an analysis of over 14 months of data from S3-3 satellite at low altitude. The majority (306) of the events occur in a narrow latitudinal zone at nightside and were embedded within a broader region of strong ion precipitation. Thorne and Andreoli attributed 302 of the events to be caused by electrostatic ion cyclotron waves(EIC waves). Only four events were believed to

be caused by EMIC waves. An example of the four events is given in Figure 3 of Thorne and Andreoli's paper. It shows isotropic electron distribution which is the sign of strong diffusion accompanied by simultaneous broader strong ion precipitation. Simultaneous EMIC wave observation was not available. As will be mentioned later in this thesis, the event reported by Thorne and Andreoli is at a boundary that looks like what other authors identified as trapping boundary even though it is at relatively low L of 4.35. Isotropic electron distribution at trapping boundary is often seen regardless of the presence of EMIC waves. Imhof et al in 1986 [20] selected 40 relativistic electron events that occurred at plasmapause crossing. The event selection criteria excludes events near trapping boundary. The occurrence rate of these relativistic electron events at plasmapause according to Imhof is one percent. Nine out of the 40 electron enhancement events come with ion precipitation at the same time and location. The electron enhancement preferentially occurs at relativistic energies of from several hundred keV to greater than 4 MeV which is consistent with the energy selective nature of EMIC wave scattering. However, Imhof pointed out that the electron flux pitch angle distribution is far from isotropic. The loss cone electron flux is at least one order of magnitude lower than electrons at 90° .

Measurement of bremstrahlung X-rays associated with relativistic electron precipitation by balloon experiments and electron spectra measurements by low Earth orbit both show preference of relativistic electron precipitation over dusk side,mostly from evening to midnight quadrant of magnetic local time [37, 9]. This agrees with what the theory suggested in 1970s by Thorne, Kennel and Lyons [47, 30]. However, satellite observations imply that the peak location of EMIC waves is in dayside mostly from late morning to early afternoon [4, 57]. Smith et al in 2016 suggest that current sheet scattering rather than EMIC wave should be studied further as a potentially important loss mechanism to account for the large amount of relativistic electron precipitation at nightside [45].

Simultaneous observations of EMIC wave activities in magnetosphere and electron precipitation provide good insight into the validity of the theory. Some authors claimed to find the evidence of electron precipitation caused by EMIC waves whereas others reported

absence of electron precipitation during the presence of strong EMIC waves. Miyoshi et al in 2008[38] reported a greater than 800 keV electron precipitation accompanied by simultaneous 30-80 keV proton precipitation observed by POES. At the same time EMIC wave was registered by ground-based magnetometer at nearby L shell. Rodger et al in 2015 [42] reported greater than 140-230 keV electron precipitation event observed by POES during a strong helium band EMIC wave event observed by Van Allen probes. Contrarily, also from POES observation, Usanova et al in 2014 [50] reported absence of precipitation during a strong EMIC event registered by both Van Allen probes and ground-based magnetometers. Engebretson et al in 2015 [12] investigated a strong(up to 25nT p-p) global scale of EMIC wave event lasting for 8 hours in UT and covering over 12 h in MLT, being observed by both Van Allen probes and GOES satellites, and multiple ground magnetometers in Antarctica near dawn, Finland at local noon, Russia in the afternoon, and Canada from duskside to midnight. During such strong and spatially large EMIC wave event, ten passes of POES satellites near footprint of Van Allen probes detected strong 30-80 keV subauroral proton precipitation indicating strong interaction of protons with EMIC waves. At the same time no enhancement of electron precipitation was observed. Both Usanova and Engebretson concluded no evidence of significant electron loss by EMIC waves was found which contradicts with what Summers in 2003 predicts from quasi-linear theory.

Case studies on associating Balloon X-rays with EMIC wave events in magnetosphere were carried out as well. Li et al in 2014 [27] found the estimated amount of X-rays from electron pitch angle scattering by EMIC waves observed by GOES is only a factor of 2.7 higher than X-ray flux observed by BARREL balloon arrays. The observations from Van Allen probes and ground stations along with some assumptions about electron spectrum distribution and electron to X-ray models were used to overcome the one L shell displacement between GOES and BARREL. Zhang et al [55] studied another conjunction case between Van Allen probes and BARREL. Since EMIC wave event is highly localized both in space and time, Zhang concluded that the X-ray event is likely associated with EMIC wave observed by Van Allen probes.

The selective pitch angle scattering by EMIC waves at low and medium pitch angle produces so called "pancake" electron distribution with electrons around 90 degree intact and electrons at lower pitch depleted. In both Usanova [50] and Engebretson [12] 's work it is found that pitch angle distribution of ultra-relativistic electrons at 2.3-5.6 MeV is more pancake-like when EMIC waves are present. The quasi-linear diffusion coefficients of EMIC wave diffusion show that higher energy electrons are confined at narrower pitch angle range centered at 90 degree. This is consistent with observation as well. Zhang XJ et al in 2016 [56] simulated time evolution of electron pitch angle distribution during a long-lasting EMIC wave event. The simulation agrees with the measurements of electrons at energy greater than 1.8 MeV and medium pitch angles but fails to reproduce the electron profile at energy lower than 1.8 MeV and small pitch angles.

In summary, observations show the pancake distribution of electrons at ultra-relativistic energy can be explained by the EMIC wave diffusion. There exists seemingly conflicting evidences of electron precipitation associated with EMIC waves[38, 42, 50, 12]. Some authors reported no evidence supporting the strong depletion of electrons by EMIC wave as predicted by the current quasi-linear theory.

1.4 Motivation, science question and outline of this thesis

The identification of loss mechanisms will help construct a good physics-based radiation belt electron model. Hiss and EMIC waves are two of the three major wave modes that had been suggested to precipitate electrons from radiation belt into Earth's atmosphere. The testing and validation of the theories have not been finished despite of some progresses made since 1970s. More work needs to be done to verify which part of the theories agree with observations and which part need to be modified to fit the observations. This thesis is to test the theories by comparing the predicted and measured electron distribution at loss cone, quantitatively evaluate the discrepancy between current quasi-linear theories of hiss and EMIC wave diffusion and observations, peek into the legitimate regime of the theories and give some guidance to the modifications of the theories.

Though there exist increasing evidences consistent with electron loss by hiss wave diffusion, a quantitative comparison of loss cone electron distribution to simultaneous hiss wave events on one-to-one correspondence is lacking. The few one-to-one correspondence study carried out using POES electron measurements and balloon X-rays mentioned in previous sections is limited by the instrument capacity. POES satellites only have two electron telescopes pointing at 0° and 90° which means it's impossible to construct electron pitch angle distribution inside loss cone which is vital for inferring diffusion by particular wave mode. The energy resolution of electron detectors onboard POES is coarse($> 30keV, > 300keV, > 1MeV$) too. POES also has electron-proton cross contamination problem. Hardman et al in 2015 [15] reported weak precipitation seen by ground-based VLF receivers but invisible to POES probably due to its small geometric factor. Though both Van Allen probes and BARREL provide high quality wave and X-ray data, the electron distribution inside loss cone can not be inferred from X-rays. The one-to-one correspondence analysis on loss cone distribution will be carried out in this thesis. About 38 cases of hiss diffusion will be analyzed. This relatively large number of cases will give more insight into the legitimate regime of hiss theory and the role of hiss waves in depleting radiation belt electrons than from the one or two cases published by other authors.

As mentioned in previous section,the strong diffusion predicted by the theory[46] suggests EMIC wave could be very important loss mechanism during magnetic storm. On the other hand, seemingly contradictory evidences of electron precipitation associated with EMIC waves have been reported from different authors. The strong capacity of electron removal predicted by theory is also being challenged by the lack of observed significant loss of electrons. The observed pancake distribution of electrons at ultra-relativistic energy gives some credit to the theory. This thesis will help to have a clearer picture of EMIC wave diffusion and the legitimacy of current theory from the perspective of electron loss cone distribution.

One of the biggest obstacles of testing either hiss or EMIC theory is lack of electron measurements at loss cone with enough energy and pitch angle resolution and simultaneous

wave measurements at high altitude magnetic equator. New space missions are needed if we are not able to unearth qualified data set from old space missions. Fortunately, during the last ten days of the prematurely dead CRRES mission in early October 1991, there are about 50 conjunctions between CRRES sitting at the vicinity of magnetic equator and UARS orbiting low Earth orbit at the magnetic footprint of CRRES. The study carried out in this thesis relies on this piece of data set.

The details about data, instrumentation and overview of UARS and CRRES missions will be presented in Chapter 2. Chapter 3 is devoted to the theoretic framework of quasi-linear diffusion theory and the customary formulas derived from quasi-linear theory for testing hiss and EMIC wave diffusion. The measured wave power is fed to a formula for computing diffusion coefficients. Full cold plasma dispersion relationship of EMIC waves is incorporated in the EMIC wave diffusion coefficient formula. Comparison of hiss diffusion to electron loss cone distribution will be presented in Chapter 4. A similar comparison for EMIC waves is in Chapter 5. Chapter 6 summarizes the entire thesis. Appendix lists more details about diffusion coefficient formulas, code implementation and testing, and misc.

Chapter 2

DATA SET

2.1 UARS satellite

2.1.1 Mission overview

The UARS (Upper Atmosphere Research Satellite) was lauched in September 12th, 1991 by Space Shuttle Discovery into a nearly circular orbit at nominal altitude of 585km with inclination of 57°. The orbit processed 5° per day relative to the Sun. Like most low Earth orbit satellites, the orbital period is about one hour and half. It was the first observatory of NASA 's Mission to Planet Earth carrying out first systematic and comprehensive study of Earth's stratosphere and mesosphere. This mission was designed to survive for three years. Six out of ten instruments functioned for more than 14 years. The official decommission was on December 14th, 2005. More details about the mission can be found in Carl Reber's introductory GRL paper[40] and NASA's UARS main science page.

2.1.2 Electron and proton instrument

Though the mission focused on atmospheric science, the Particle Environment Monitor (PEM) on board UARS provided quality measurements of radiation belt electrons and protons with high energy and pitch angle resolutions. At most of the time when UARS is at the footprint of outer radiation belt, there are three electron telescopes well inside bounce loss cone and one right outside loss cone. For testing wave-particle theory with loss cone distribution, UARS PEM provides so far the best data set compared to existing or past missions such as POES, SAMPEX and some cubsat missions.

PEM consists of four instruments: the atmospheric X-ray imaging (AXIS), vector mag-

netometer (VMAG), medium particle spectrometer (MEPS) and high energy particle spectrometer(HEPS). HEPS electron and proton data is used for the research on radiation belt electron in this thesis. The satellite is three-axis stabilized. There are four HEPS telescopes mounted at zenith each with a 15°half cone angle facing upward hemisphere. There are two telescopes at nadir looking at the Earth (see 2.1). HEPS electron detectors measure electrons from 30 keV to 5 MeV at 32 energy bins. The energy bin size is 15 keV at low energy and 100 keV at high energy. The relatively large geometric factor of 0.54 cm^2sr makes it possible to see low precipitating flux. For more details about PEM and HEPS ,see J.D. Winningham's instrument paper[54]. Level 2 HEPS electron data in binary format with time resolution of

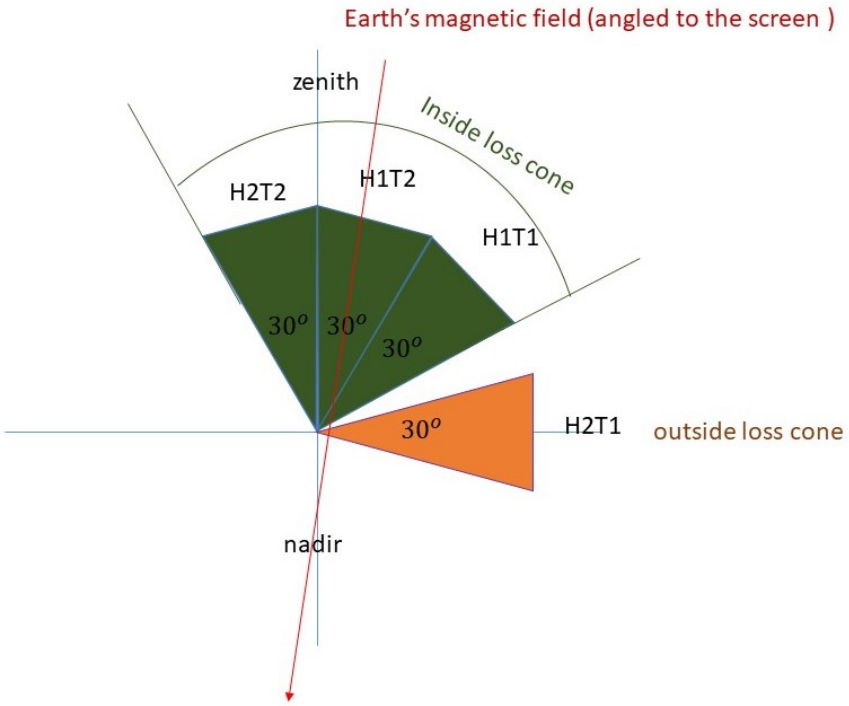

Figure 2.1: Orientation of UARS HEPS electron telescopes

4.086 s used in this thesis can be located at website hosted by NASA Goddard flight center (`https://mirador.gsfc.nasa.gov/`) with searching keyword of "UARS HEPSA" . The

IDL code modified from the code provided by Dr W Dean Pesnell for reading the binary data is attached in the appendix. The PEM data can also be plotted and downloaded from Southwest Research Institute Virtual Sun/Earth Observatory (`http://vseo.space.swri.edu/`) with customary data format. The first set of HEPS data became available on Oct 1st, 1991.

2.2 CRRES satellite

2.2.1 Mission overview

The CRRES (Combined Release and Radiation Effects Satellite) was launched on July 25, 1990 from Cape Canaveral Air Force Station by Atlas I. The mission was planned for three years but communications lost on early morning of October 12, 1991. The initial orbit was 350 by 33,584km with an inclination of 18.1° and orbital period of 613.4 minutes. The orbit is similar to the double Van Allen probes launched in August 2012. The spacecraft traversed the heart of outer equatorial radiation belt slowly at its apogee. For more details about CRRES mission , please read M.H.Johnson's paper [22] and other online resources.

2.2.2 Electron instrument

The CRRES MEA (Magnetic Electron Spectrometer) utilizes the principal of momentum analysis in a solenoid magnetic field to measure electrons spectrum. The electrons are bent by uniform magnetic field by 180° before hitting the detector array. It measures electrons at center energy from 153 to 1582 keV with 18 energy bins. The angular resolution at different energy bins varies from 2.82° to 16.48°. In the data set used in this thesis there are 19 pitch angle bins with equal size of 5° from 0° to 90°. The time resolution is 25 s.The MEA electron spectrum is used to for comparison to the EMIC wave scattering at equatorial radiation belt. The CDF format MEA electron data is accessible at `ftp://spdf.gsfc.nasa.gov/pub/data/crres/particle_mea/mea_h0_cdaweb/1991/`. For more information about MEA read the instrument paper by Vampola [52].

2.2.3 Wave instrument

The CRRES PWE(Plasma Wave Experiments) provides measurements of electric fields from 5.6 Hz to 400kHz and magnetic fields from 5.6 Hz to 10kHz with a dynamic range of at least 100 dB. The module consists of three sensors: 1) a 100m tip-to-tip electric dipole antenna 2) a search coil magnetometer 3) a 94m sphere-to-sphere double probe electric antenna. The instrument paper by Roger Anderson from University of Iowa provides more details about PWE [5]. Like the data from most of instruments of CRRES mission, PWE data is not archived. Our research relies on two data sources: 1) the CDF files that seem to be cooperative product by French aerospace lab (ONERA) and PWE PI Roger Anderson, 2) gif plots of waves activities from University of Iowa. The CDF files provide cold plasma density, electron gyro-frequency, electric field and magnetic field wave power above 100Hz. The pixels of gif plots are converted into electric wave power according to the color bars. The gif-generated electric field wave power extends to frequency below 100Hz. The CDF files and gif plots can be obtained from Physics Department of University of Iowa.

2.2.4 Magnetometer

The fluxgate magnetometer on board CRRES was to measure both Earth's magnetic field and ultra low frequency waves such as EMIC waves at Pc 1and 2 bands and Pc3-5 Alfvenic ULF waves. It also provides the pitch angle for particle instruments. The magnetometer 's dynamic range goes from a fractional to 48,000 nanotesla. The resolution is 0.07 nT at high gain and 3.3 nT at low gain mode. For ULF wave measurement, the noise level at high sensitivity is about $2 \times 10^{-3}\ nT^2Hz^{-1}$. The EMIC wave spectrogram processed from magnetometer data used in this thesis is provided by Dr Nigel Meredith in British Antarctic Survey who might obtained the data from emeritus Prof. Brian Fraser from University of Newcastle. A list of identified EMIC wave events compiled by Brian Fraser is obtained by the author of this thesis from Dr Nigel Meredith too.

2.3 UARS and CRRES magnetic conjunction

The UARS overlapped with CRRES in the first eleven days of October 1991 before CRRES was lost in early October 12. There are more than 50 conjunctions during this period. About 38 conjunction cases were analyzed. The rest 12 cases were not analyzed due to the lack of either hiss wave data or cold plasma density data. EMIC waves were observed at three conjunctions.

A conjunction occurs when the two spacecraft 's sitting approximately at the same magnetic field tube at the same time as shown by the schematic view of Figure 2.2. The spatial closeness is defined in terms of McIlain L-shell and magnetic local time. It is arbitrarily decided that UARS and CRRES are at conjunction when they are within 0.2L and 1 hour magnetic local time from each other (within one exception of 0.3L and 1.2 hour) . This criteria is not largely different from that has been used by other scientists and tighter than 0.5L or even 1L by some authors[27]. A conjunction event typically lasts for 50 to 60 seconds. All the conjunctions occur when UARS is at northern hemisphere and CRRES is near the magnetic equator. The temporal and spatial distribution of all 38 conjunctions are given by 2.3 and 2.4

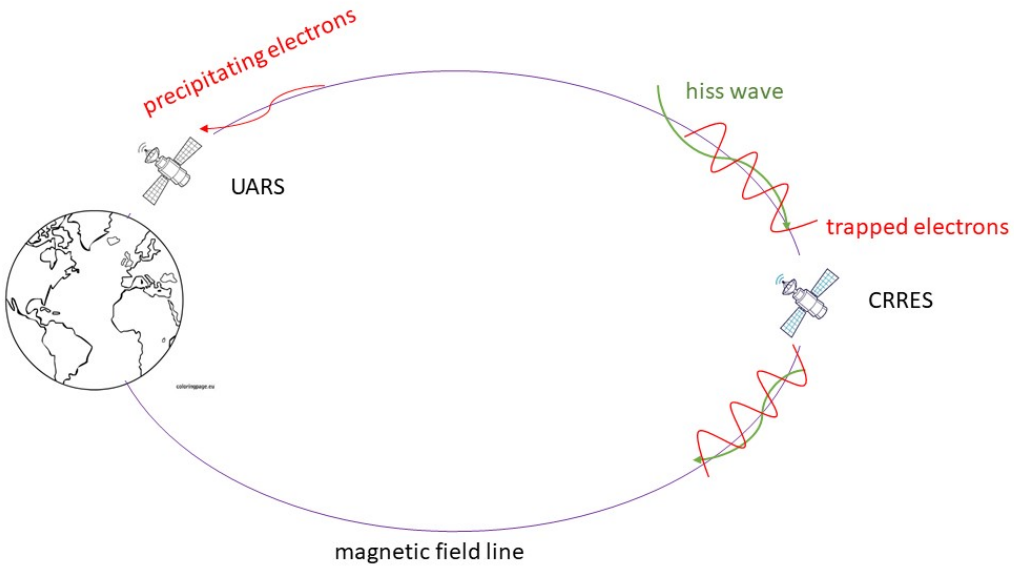

Figure 2.2: schematic view of a magnetic conjunction between UARS at 585km and CRRES at about 33,000km magnetic equator.

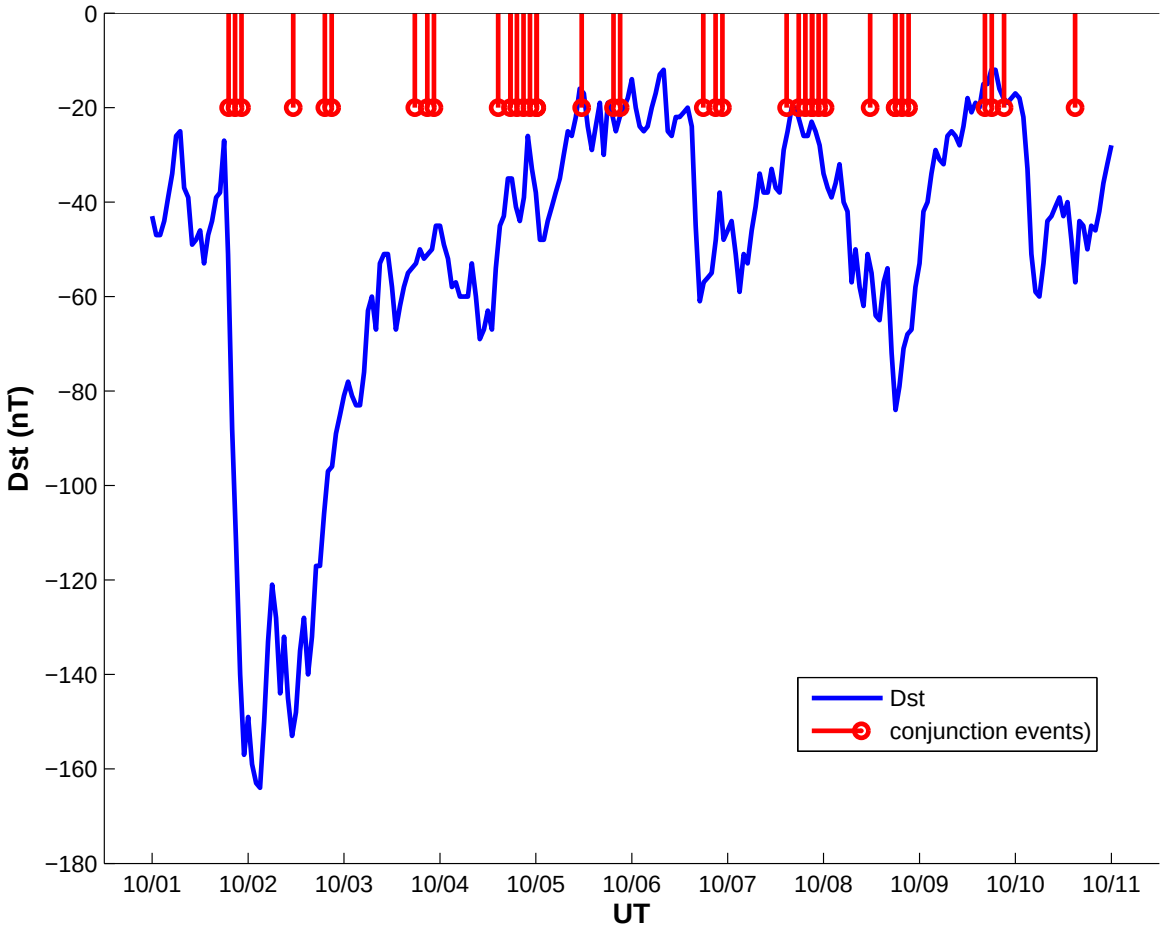

Figure 2.3: Temporal distribution of 38 conjunction cases in Oct 1991.

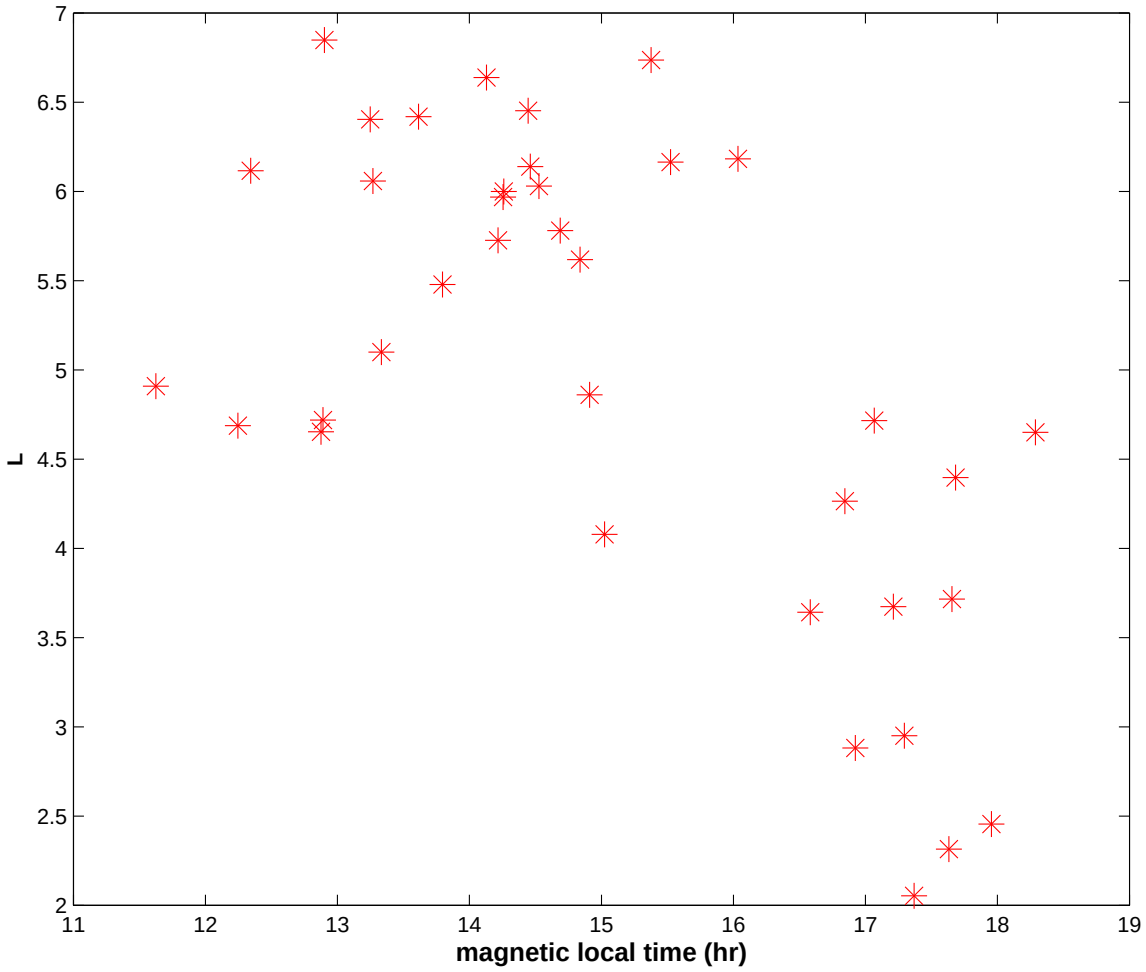

Figure 2.4: Spatial distribution of 38 conjunction cases in Oct 1991.

Chapter 3

THEORETIC FRAMEWORK OF QUASI-LINEAR DIFFUSION

The formulas needed for comparison of hiss and EMIC wave theory to the observed electron distribution at loss cone are derived from quasi-linear theory in this chapter. The solution of electron distribution function at steady state given by Kennel and Petschek in 1960s will be reviewed and followed by a brief proof for extension to non-steady state. New diffusion coefficients formulas for both hiss and EMIC wave are derived from quasi-linear theory at a cold plasma. Compared to the conventional formulas used in Lyons et al 1972[32], the assumptions of Gaussian wave frequency is dropped while the Gaussian wave normal angle distribution is preserved.

3.1 Wave-particle interaction as a diffusion process

The theories from 1960s state the wave-particle interaction is a diffusion process described by diffusion equation. The Lorentz force of wave field scatter particles reducing the gradient of particle distribution on pitch angle or energy space. The magnitude of diffusion coefficient is determined by the wave properties. If wave frequency is relatively low and particle energy is high, energy diffusion is negligible and only pure pitch angle diffusion is considered. This assumption is valid for hiss and EMIC wave scattering.

3.1.1 Existing solution of loss cone distribution function at steady state

Kennel and Petschek in 1966 [24] first proposed that the existence of loss cone makes a sharp gradient of electron distribution at the vicinity of loss cone which generates whistler mode electron cyclotron waves. The waves smooth out the gradient by pushing trapped electrons into loss cone. The wave growth rate depends on both the magnitude of gradient and number

of electrons at resonance. The wave growth rate decreases as gradient decreases. That is called electrons being dumped into atmosphere by self-generated waves. At steady state by assuming a source of particles balancing the loss and a reasonable wave damping rate, Kennel and Petschek's diffusion equation for electrons inside loss cone at equatorial magnetosphere is written as

$$\frac{1}{\alpha_0}\frac{\partial}{\partial\alpha_0}\left(D^*\alpha_0\frac{\partial f}{\partial\alpha_0}\right)=\frac{f}{T_E} \tag{3.1}$$

where f is phase space density as function of equatorial pitch angle α_0 at constant energy. The right hand side term is loss to the atmosphere. T_E is quarter bounce period. It's assumed that there is no source inside loss cone and diffusion coefficient D^* is constant due to small value of α_0. The small size of loss cone at the equator implies $\sin(\alpha_0)\approx\alpha_0$. Equation 3.1 can be transformed into modified Bessel equation with variable manipulation. As will be shown later, the solution inside loss cone is modified Bessel function first kind. The diffusion outside loss cone is written as

$$\frac{1}{\sin\alpha_0}\frac{\partial}{\partial\alpha_0}\left(D\sin\alpha_0\frac{\partial f}{\partial\alpha_0}\right)=-s(\alpha_0,v) \tag{3.2}$$

where D is diffusion coefficient, $s(\alpha_0,v)$ is source term. It's assumed there is no additional loss outside loss cone. By requiring finite electron flux at the center of loss cone, assuming continuity of f and its derivative at the edge of loss cone and $f'\left(\frac{\pi}{2}\right)=0$, an analytical solution inside loss cone is obtained

$$f(\alpha_0,v)=\frac{S(v)}{D^*}h(\alpha_0)=\frac{S(v)}{D^*}\frac{\sqrt{D^*T_E}}{\alpha_c}\frac{I_0(\alpha_0/\sqrt{D^*T_E})}{I_1(\alpha_c/\sqrt{D^*T_E})} \tag{3.3}$$

where α_c is size of loss cone , D^* diffusion coefficient inside loss cone, $S(v)$ is integration of source term over pitch angle, I_0 and I_1 are zeroth and first order modified Bessel function of first kind. The solution outside loss cone is given by

$$f(\alpha_0,v)=\frac{S(v)}{D^*}\left\{h(\alpha_c)+\ln\frac{\sin\alpha_0}{\sin\alpha_c}\right\} \tag{3.4}$$

To obtain 3.4, it is assumed that $D(\alpha_0)=D^*/\cos\alpha_0$ which is a good approximation at small and medium pitch angles.

3.1.2 Extension of steady state solution to non-steady state

Kennel and Petschek's theory can not explain the very low flux of electrons at the slot region since the electron flux is too low to be able to self generate waves. Lyons , Thorne and Kennel in 1972[32] suggested whistler mode hiss wave filled with the entire plasmasphere can scatter radiation belt electrons to very low flux. Since hiss wave is generated by a different group of electrons rather than the electrons being scattered, it is called parasitic diffusion. Research shows chorus wave and lightning contribute as source of hiss wave too. In the same year, Lyons and Thorne [30] proposed EMIC wave is able to parasitically diffuse radiation belt electrons at fast pace due to it large amplitude. One thing we need to keep mind is that diffusion means gradient is being reduced and the distribution function is relaxed. That is true even for parasitic diffusion.

Attaining a steady state is not guaranteed in the parasitic diffusion by hiss and EMIC waves. The electrons loss might not be replenished especially in the slot region. The balance between wave damping and growth is not guaranteed either. A non-steady state solution of loss cone distribution is needed. In this section, I will prove that solution of loss cone distribution can be obtained by slightly tweaking the steady-state solution.

The non-steady state diffusion equations are given by 3.5 and 3.6. Roberts in 1969[41] found that any arbitrary pitch angle distribution that might result from an injection event will soon decay to the lowest mode which is very similar to the steady state. In other words, at non-stead state, the shape of distribution function f over pitch angle space is approximately constant. The electron flux will see an exponential decay with a characteristic time determined by the magnitude of diffusion coefficient which depends on the strength of waves. That makes it possible to use separable variable method to solve equations 3.5 and 3.6 by assuming $f(\alpha_0, t) = F(t)g(\alpha_0)$. Equation 3.5 become 3.7, where τ is called electron life time.

$$\frac{\partial f}{\partial t} = \frac{1}{\alpha_0}\frac{\partial}{\partial \alpha_0}\left(D\alpha_0\frac{\partial f}{\partial \alpha_0}\right) - \frac{f}{T_E}, \alpha_0 < \alpha_c \tag{3.5}$$

$$\frac{\partial f}{\partial t} = \frac{1}{\sin\alpha_0}\frac{\partial}{\partial\alpha_0}\left(D\sin\alpha_0\frac{\partial f}{\partial\alpha_0}\right), \alpha_0 > \alpha_c \tag{3.6}$$

$$\frac{\mathrm{d}F}{\mathrm{d}tF\left(t\right)} = \frac{1}{g\sin\alpha_0}\frac{\mathrm{d}}{\mathrm{d}\alpha_0}\left(D\sin\alpha_0\frac{\mathrm{d}g}{\mathrm{d}\alpha_0}\right) - \frac{1}{T_E} = -\frac{1}{\tau} \tag{3.7}$$

Right hand side of 3.7 is essentially a zeroth-order modified Bessel equation and rewritten as 3.8. The solution is zeroth-order modified Bessel function of first kind (equation 3.9). The pitch angle function $h(\alpha_0)$ in the solution is different from 3.3 only by small modification from τ. As the theory says [30] at small pitch angle τ is approximately reciprocal of diffusion coefficient. The diffusion coefficient of a typical hiss wave is less than $10^{-3}s^{-1}$. At the strong diffusion $D = \frac{\alpha_0^2}{2T_E}$ [49]. Under any situation D is at least two orders of magnitude smaller than $\frac{1}{T_E}$. Therefore $h(\alpha_0)$ in equation 3.9 become identical as that in 3.3.

$$u^2\frac{\mathrm{d}^2 g}{\mathrm{d}u^2} + u\frac{\mathrm{d}g}{\mathrm{d}u} - u^2 g = 0 \tag{3.8}$$

where $u = \alpha_0/\sqrt{DT_E^{'}}$, and $\frac{1}{T_E^{'}} = \frac{1}{T_E} - \frac{1}{\tau} = \frac{1}{T_E} - D = \frac{1}{T_E} - \frac{\alpha_0^2}{2T_E} \approx \frac{1}{T_E}$

$$f(\alpha_0, v) = X(v)h(\alpha_0) = \frac{X(v)}{\frac{\alpha_c}{\sqrt{D^*T_E^{'}}}}\frac{I_0(\alpha_0/\sqrt{D^*T_E^{'}})}{I_1(\alpha_c/\sqrt{D^*T_E^{'}})} \tag{3.9}$$

where $X(v)$ is a constant at given energy and determined by boundary conditions at the edge of loss cone.

Equations 3.3 and 3.9 show that the pitch angle shape of loss cone distribution can be completely determined by diffusion coefficients from waves whereas the knowledge about electrons outside loss cone is needed to determine the scale of the loss cone population. In a steady state when source equals loss the source term $S(v)$ in 3.3 can be estimated by by integrating the observed electron flux from the three UARS telescopes well inside loss cone (see appendix for more details). As will be shown in Chapter 4, steady state is a good assumption for the hiss waves which diffuse electrons slowly and have small fluctuation for relatively long time. Equation 3.3 along with source estimation is used for hiss wave investigation. The steady state might not be a good assumption for EMIC waves which

cause strong diffusion and last for short time, equation 3.9 is used instead and the scale factor $X(v)$ is determined by the electron flux right outside loss cone assuming continuity of distribution function across loss cone and the pitch angle shape preservation at non-steady state.

3.2 Formula of pitch angle diffusion coefficient

Diffusion coefficient along with proper boundary conditions are essential to solve the diffusion equations. The bounce-averaged pitch angle diffusion coefficient formulas for hiss and EMIC waves developed by Lyons in 1970s [32, 29] from cold plasma quasi-linear diffusion theory have been widely used for several decades. The wave frequency distribution was assumed to be a Gaussian distribution with lower and upper frequency cutoff. The real wave power spectrum is rarely to be Gaussian. One Gaussian fit could deviate the real wave distribution largely. Multiple Gaussian fit was used to fit wave power spectrum by some authors [34]. It has to been done manually for each spectrum and good fit is not always guaranteed. To avoid this cumbersome work in this thesis new formulas of diffusion coefficients for both hiss and EMIC waves are derived. The measured wave power spectra is fed to the algorithm without any pre-processing of wave power with curve fitting. The rest of this section will start with the relativistic quasi-linear diffusion theory from Lyons, Thorne and Kennel's work in 1970s [28, 32, 29] and walk through the process of deriving new formulas. A brief description of MATLAB code implementation and testing is in the appendix. Contact the author for MATLAB code.

In resonant diffusion and low frequency limit the relativistic quasi-linear diffusion equation is reduced to a simple form [28] given by

$$\frac{\partial f}{\partial t} = \frac{1}{\sin\alpha}\frac{\partial}{\partial\alpha}\Big(\sum_{n=-\infty}^{\infty} D_n\Big)\sin\alpha\frac{\partial f}{\partial\alpha} \tag{3.10}$$

for $n \neq 0$

$$D_n = \lim_{V\to\infty}\frac{\pi e^2}{V(2\pi)^2\gamma m P_\parallel}\int_0^\infty k_\perp dk_\perp\big[\big(\frac{k_\parallel}{\omega_{\mathbf{k}}}\big)^2\big|\theta_{n,\mathbf{k}}\big|^2\big]\;|_{k_\parallel=-n\Omega m/P_\parallel} \tag{3.11}$$

where V is volume of plasma, γ is relativistic factor, $P_{\|}$ is parallel momentum of particles, n is harmonic number, m is electron rest mass, Ω is electron gyro-frequency, $\mathbf{k}$ and ω are wave vector and frequency, the $\theta_{n,\mathbf{k}}$ is function of wave electric field given by

$$\theta_{n,\mathbf{k}} = \frac{E_{\mathbf{k},R}J_{n+1} + E_{\mathbf{k},L}J_{n-1}}{\sqrt{2}} + \frac{v_{\|}}{v_{\perp}}E_{\mathbf{k},\|}J_n \tag{3.12}$$

where $E_{\mathbf{k},\|}$ is electric field component parallel to background magnetic field, the perpendicular electric field is expressed in terms of right hand $E_{\mathbf{k},R}$ and left hand $E_{\mathbf{k},L}$ components, $v_{\|}$ and $v_{\perp}$ are particle parallel and perpendicular velocities, the argument of first kind Bessel function J_n is $k_{\perp}P_{\perp}/m\Omega$, Ω is the particle gyro-frequency. $E_{\mathbf{k},R}$, $E_{\mathbf{k},L}$ and $E_{\mathbf{k},\|}$ can be expressed in terms of wave magnetic power $|B_{\mathbf{k}}|^2$ in $\mathbf{k}$ space by using cold plasma relation. Since the measured wave power is usually in frequency space, $|B_{\mathbf{k}}|^2$ is further converted to wave power B_{ω}^2 as function of frequency assuming (see Lyons' papers [28, 29])

$$|\mathbf{B}_{\mathbf{k}}|^2 = \frac{V}{N(\omega)}B^2(\omega)G_{\omega}(\theta) \tag{3.13}$$

where $N(\omega)$ is the normalization factor, V is plasma volume, $G_{\omega}(\theta)$ is wave normal angle distribution. Though the ω in $G_{\omega}(\theta)$ implies the wave frequency dependency of wave normal angle distribution, in this thesis wave normal angle distribution is assumed to be the same over all wave frequencies by following Lyons' method. In the rest part of the thesis, the ω notation will be dropped from wave normal angle term .The formulas of $N(\omega)$ for both hiss and EMIC wave are given in the appendix.

3.2.1 Hiss wave bounce-averaged pitch angle diffusion coefficient

For whistler wave with moderate wave normal angle and frequency between electron and proton gyro-frequencies, with a greatly simplified dispersion relationship (3.14) used by Lyons and other authors [28, 29, 35], The electric field $\theta_{n,\mathbf{k}}$ is a related to $|\mathbf{B}_{\mathbf{k}}|^2$ by 3.15

$$\mu^2 = \frac{c^2k^2}{\omega^2} = \frac{\omega_{pe}^2}{\omega\Omega_e\cos(\theta)} \tag{3.14}$$

where ω_{pe}^2 is plasma frequency,k and ω are magnitude of wave vector and angular frequency, Ω_e is electron gyro-frequency, θ is wave normal angle, c is speed of light in vaccum.

$$|\theta_{n,\mathbf{k}}|^2 = \frac{|\mathbf{B_k}|^2}{8c^2}\left(\frac{\omega_\mathbf{k}}{k_\parallel}\right)^2\left\{(1+cos\theta)J_{n+1}+(1-cos\theta)J_{n-1})\right\}^2 \tag{3.15}$$

where c is vacuum speed of light, θ is wave normal angle, The argument of firs kind Bessel function J_v is $k_\perp P_\perp/m\Omega_e$, $|\mathbf{B_k}|^2$ is the wave power on k space.

By plugging 3.15, 3.13 and A.6 into 3.11, transferring from $\mathbf{k}$ space to ω and X (tangent of wave normal angle) space, and evaluating all terms at resonance condition of $k_\parallel = -n\Omega m/P_\parallel$, 3.11 is rewritten as

$$D_n = \frac{\pi|n|e^2\Omega_e^2}{8\gamma P_\parallel^2\omega_{pe}^2 I}\int_{X_{min}}^{X_{max}} dX\frac{X}{(1+X^2)^{\frac{1}{4}}}B^2(\omega)g(X)\Phi_n(X) = \frac{\pi|n|e^2\Omega_e^2 I_n}{8\gamma P_\parallel^2\omega_{pe}^2 I} \tag{3.16}$$

where I is defined in appendix A.6, $\Phi_n(X) = \left\{(1+cos\theta)J_{n+1}+(1-cos\theta)J_{n-1})\right\}^2$, X_{min} and X_{max} are determined by resonance condition, dispersion relationship and the frequency range of hiss waves, the integral is replaced by I_n for compactness, wave frequency ω is evaluated via dispersion relationship and resonance condition at each value of X, $B^2(\omega)$ is measured wave power spectrum. $g(X)$ is wave normal angle distribution. The diffusion coefficient at loss cone is insensitive to wave normal angle models[14]. A Gaussian normal angle distribution centered at zero degree with width of 80° is adopted. The cyclotron resonance diffusion coefficient at given local pitch angle α can be obtained by summing 3.16 over harmonics as following

$$D(\alpha) = \frac{\pi e^2\Omega_{eq}^2 h^2(\lambda)}{8\gamma P^2 cos^2\alpha\omega_{pe}^2 I(\lambda)}\sum_n |n|I_n(\lambda,\alpha) \tag{3.17}$$

where in this thesis the highest harmonic computed is $|n| = 5$, the contribution from harmonics higher than 5 is negligible as demonstrated by Lyons and other authors[32], local electron gyro-frequency Ω_e is related to equatorial gyro-frequency Ω_{eq} by latitude λ dependent term $h(\lambda)$, for Earth's dipole field $h(\lambda)$ is given by

$$h(\lambda) = \frac{(1+3\sin^2\lambda)^{\frac{1}{2}}}{cos^6\lambda} \tag{3.18}$$

According to Lyons' work [32], the bounce-averaged diffusion coefficient can be evaluated over magnetic latitude and is related to local pitch angle diffusion coefficient by

$$D(\alpha_0) = \frac{1}{T(\alpha_0)} \int_0^{\lambda_m} D(\alpha) \frac{cos\alpha}{cos^2\alpha_0} cos^7\lambda d\lambda \tag{3.19}$$

where α_0 is equatorial pitch angle, $T(\alpha_0) = 1.30 - 0.56\sin(\alpha_0)$, λ_m is minimum of particle bouncing mirroring latitude and latitude where waves are reflected back to equator. For hiss wave the reflecting latitude is believed to be around 45°. The diffusion coefficient at loss cone is insensitive to change of λ_m from mirroring latitude to 45°. Finally, the bounce-averaged pure pitch angle diffusion coefficient is written as

$$D(\alpha_0) = \frac{\pi e^2 \Omega_{eq}^2}{8\gamma P^2 \omega_{pe}^2} \frac{1}{cos^2\alpha_0 T(\alpha_0)} \int_0^{\lambda_m} d\lambda \frac{cos^7\lambda h^2(\lambda)}{[1 - h(\lambda)\sin^2\alpha_0]^{\frac{1}{2}} I(\lambda)} \sum |n| I_n(\lambda, \alpha) \tag{3.20}$$

3.2.2 EMIC wave bounce-averaged pitch angle diffusion coefficient

The full dispersion relationship of EMIC wave (see Albert 2003 [3]) is given by

$$\mu^2 = \frac{c^2k^2}{\omega^2} = \frac{\omega_{pe}^2}{\Omega_e^2} \frac{1}{\Psi} \tag{3.21}$$

by normalizing wave frequency over proton gyro-frequency, it is rewritten as

$$\frac{M^2\omega_{pe}^2}{k_\parallel^2 c^2} Y^2 = \Psi(X, Y) \tag{3.22}$$

where M is electron-to-proton mass ratio, X is tangent of wave normal angle, $Y = \omega/\Omega_p$ is wave frequency over proton gyro-frequency. For one value of X, the resonant Y has three values with one in each of the three ion bands(Hydrogen, Helium and Oxygen). By using similar notations used by Albert[3] Ψ is given by

$$\Psi(X, Y) = AX^2 + \frac{1}{2}(\frac{1}{R} + \frac{1}{L})(1 + X^2) \pm (-Sign(L))(A^2X^4 + B^2(1 + X^2))^{\frac{1}{2}} \tag{3.23}$$

where $A = \frac{1}{2}\left[\frac{1}{P} - \frac{1}{2}\left(\frac{1}{L} + \frac{1}{R}\right)\right]$, $B = \frac{1}{2}\left[\frac{1}{L} - \frac{1}{R}\right]$, R, L and P are Stix's cold plasma wave coefficients normalized by ω_{pe}^2/Ω_e^2 and given by

$$R = \frac{1}{M} \sum_i \frac{\eta_i \beta_i}{1 + \beta_i Y/Z_i} \tag{3.24}$$

$$L = \frac{1}{M}\sum_i \frac{\eta_i \beta_i}{1-\beta_i Y/Z_i} \tag{3.25}$$

$$P = -\frac{1}{(MY)^2}\left[1 + M\sum_i \eta_i Z_i^2/\beta_i\right] \tag{3.26}$$

where $\beta_i = m_i/m_p$ is ion-to-proton mass ratio, $\eta_i = n_i/n_e$ is ion-to-electron density ratio, Z_i is charge number. The summation is over ion species with electron excluded. The relative proportion of ion species affect the bands of EMIC waves through R,L and P terms. A $70\%H+$,$20\%He+$ and $10\%O+$ is adopted for magnetic storm time ion proportion as followed by convention[3]. The electric field $\Theta_{n,\mathbf{k}}$ in 3.12 is related to magnetic field power via cold plasma relation and given by

$$|\theta_{n,\mathbf{k}}|^2 = \frac{|B_{\mathbf{k}}|^2}{\mu^2}|\Phi_{n,\mathbf{k}}|^2 \tag{3.27}$$

where $|\Phi_{n,\mathbf{k}}|^2$ is given by

$$|\Phi_{n,\mathbf{k}}|^2 = \frac{1}{4}\left[A_{n+1}J_{n+1} + A_{n-1}J_{n-1}\right]^2 \tag{3.28}$$

The coefficients in front of Bessel function J_v are functions of X and Y through dispersion relationship and given by

$$A_{n\pm1} = \pm\frac{\left(X^2 + \frac{\omega_{pe}^2}{c^2k_\parallel^2}\right)\frac{D}{\mu^2-S} + \frac{\omega_{pe}^2}{c^2k_\parallel^2}}{\sqrt{\left(\frac{D}{\mu^2-S}\right)^2\left(X^2+\frac{\omega_{pe}^2}{c^2k_\parallel^2}\right)^2 + \left(\frac{\omega_{pe}^2}{c^2k_\parallel^2}\right)^2}} \tag{3.29}$$

where

$$\frac{D}{\mu^2-S} = \frac{Y + \sum_i \frac{\eta_i Y}{(\beta_i Y)^2-1}}{\frac{c^2k_\parallel^2(1+X^2)}{M\omega_{pe}^2} + \sum_i \frac{\beta_i\eta_i Y^2}{(\beta_i Y)^2-1}} \tag{3.30}$$

By plugging 3.27 into 3.11 and using similar manipulation from hiss diffusion coefficient derivation, the local pitch angle diffusion coefficient from EMIC wave scattering is given by

$$D(\alpha) = \sum_{n\neq0} D_n = \frac{m_e e^2 \Omega_{eq}^2}{4\pi\gamma c^2 P^3}\frac{h^2(\lambda)}{cos^3(\alpha)}\sum_{n\neq0} n^2 I_n \tag{3.31}$$

where

$$I_n = \int_{X_{min}}^{X_{max}} X dX \left[\frac{B^2(Y) g(X) \left| \Phi_{n,\mathbf{k}} \right|^2}{N(Y)(1+X^2)} \right]_{k_\parallel = -\frac{n m_e \Omega_e}{P_\parallel}} \tag{3.32}$$

The normalization factor $N(Y)$ is given in the appendix, X_{min} and X_{max} determined by resonance condition, dispersion relationship and frequency range of EMIC waves. The bounce-averaged diffusion coefficient of EMIC wave pitch angle scattering is finally given by

$$D(\alpha_0) = \frac{\pi m_e e^2 \Omega_{eq}^3}{\gamma M^2 \omega_{pe}^2 P^3} \frac{1}{T(\alpha_0) \cos^2(\alpha_0)} \int_{\lambda_{min}}^{\lambda_{\lambda_{max}}} d\lambda \cos^7(\lambda) \frac{h^3(\lambda)}{1 - \sin^2(\alpha_0) h(\lambda)} \sum_n n^2 I_n \tag{3.33}$$

where λ_{min} is usually zero from the equator, λ_{max} depends on both resonance condition and wave latitude distribution. In this thesis, the most conservative choice of 8° is adopted for λ_{max} according to Fraser and Nguyen 's findings that all EMIC wave polarization are seen within 8° of magnetic equator whereas linear polarization dominates over $20 - 30^\circ$ latitude[13]. A more relaxed latitude model gives larger diffusion coefficient.

Chapter 4

COMPARISON OF HISS WAVE DIFFUSION THEORY TO ELECTRON LOSS CONE DISTRIBUTION

About 38 conjunction cases are analyzed for testing hiss diffusion theory. The RMS hiss amplitude varies from a few picotesla to about 120 picotesla as will be shown in later sections. Steady state is assumed if hiss wave has been present and fluctuates less than one percent in a time window that is at least twice longer than a typical conjunction time of 50-60 seconds. The hiss wave is qualitatively identified by the broad band waves spreading from tens to 1-2 kHz above $10^{-9} nT^2 Hz^{-1}$ when CRRES is traversing outer radiation belts (see Figure 4.1). Since the wave normal angle information is missing, it is unclear if there is some magnetosonic wave mixed in hiss at the low end frequency of tens of hertz.

Hiss wave has been known to fill the entire plasmasphere [32]. Here it is assumed that hiss wave exist over all latitude. Three wave normal angle models are used. The first model assumes hiss wave normal angle is a Gaussian distribution (0° center, 80° width). The second model assumes center of the Gaussian increases with latitude linearly. The wave normal angle becomes approximately 90° at latitude of 45°. The third model also assumes center of Gaussian increasing with latitude but more slowly. The wave normal angle approaches 90° at mirroring latitude. The parallel model has been used widely [32, 36]. The second model is based on some observations that hiss becomes very oblique and bounce back at about latitude of 45° [14]. The third model is tried since hiss can be observed at aurora altitude[33].

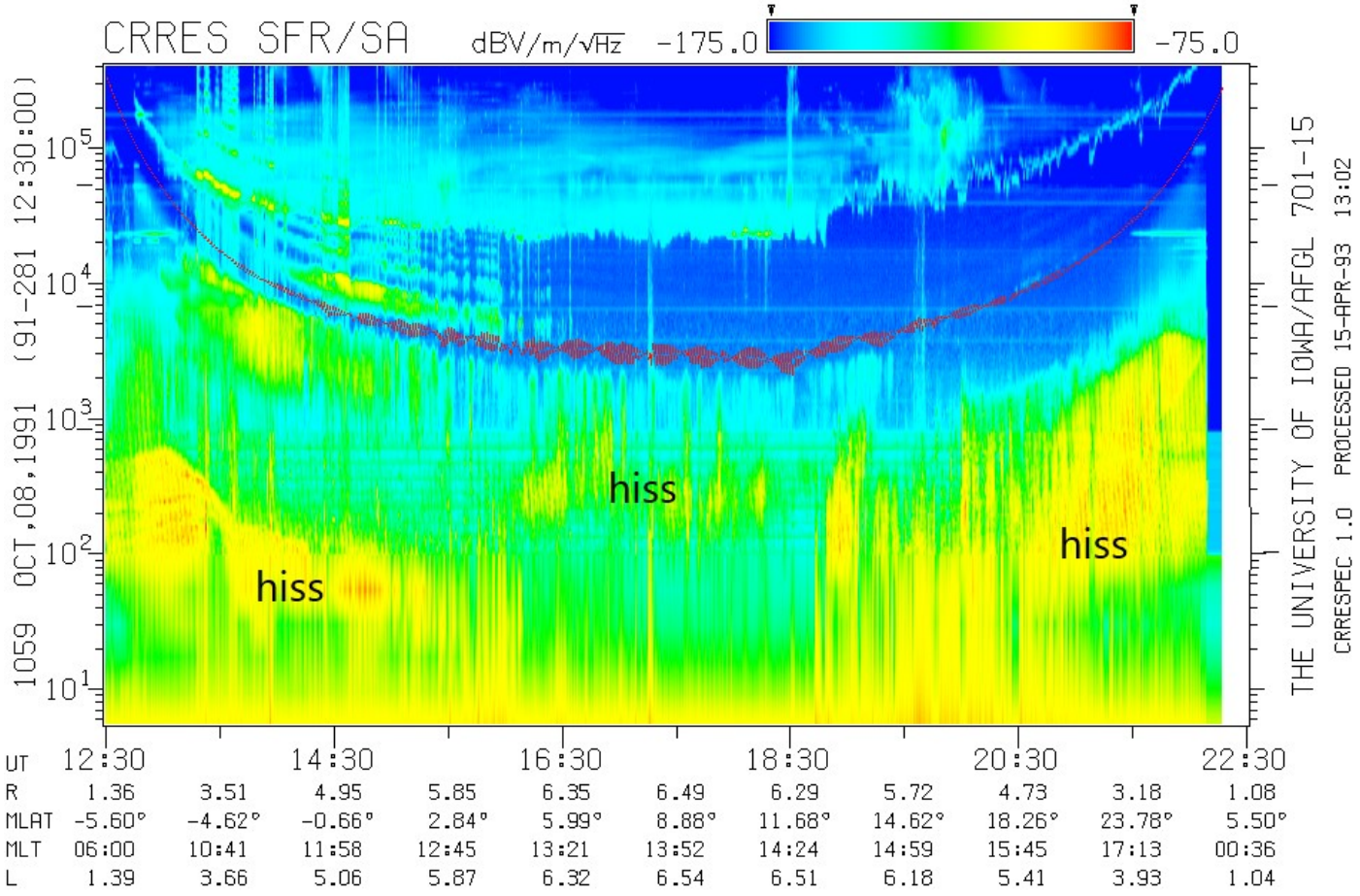

Figure 4.1: Survey plot of wave power spectrum from CRRES PWE (Plasma Wave Experiment) on Oct 8th, 1991, Orbit 1059. The plot is provided by Physics Department , University of Iowa. Th broad band hiss is typically from tens of Hz to 2 kHz. The red line is electron cyclotron frequency.

4.1 Electron precipitation events consistent with hiss diffusion

Figure 4.1 is a survey plot of electric field component of plasma wave from a few Hz to several kHz. The broad band whistler mode hiss is labeled. At universal time 21:15:00 - 21:15:54, UARS is at footprint of CRRES. The wave power spectrum at the conjunction window is plotted in Figure 4.2. The total RMS wave amplitude is about 120 pT. The wave power along with cold plasma density, L shell and electron energies are fed to the hiss diffusion coefficient formula in Chapter 3 to compute quasi-linear diffusion coefficients using three different latitude models. It turns out that diffusion at loss cone is insensitive to latitude model. The diffusion coefficients at loss cone from parallel model are $0.0022s^{-1}$ at 100 keV, $8.8 \times 10^{-4}s^{-1}$ at 500 keV and $2.4 \times 10^{-4}s^{-1}$ at 1 MeV.

A comparison of hiss diffusion curve to measured electron distribution at loss cone is given by Figure 4.3. The hiss curve is given by 3.3 in Chapter 3. The three similar panels (a), (b) and (c) are for 100 keV, 500keV and 1MeV electrons respectively. The thick blue curve is electron flux predicted by hiss diffusion theory given by equation 3.3. Under steady state, the source equals loss. The source term is estimated by adding the amount of electrons seen by three UARS telescopes inside loss cone. The red stars are measured electron flux with horizontal error bar indicates the field of view of each telescope. The pitch angle at low Earth orbit to transformed to equatorial value using equation of conservation of first adiabatic variant which relates electron pitch angles at different points along dipole magnetic field line. The black stars are obtained by integrating the blue curve over field of view of each telescope for direct comparison to red stars. The dash blue curve is just shift of thick blue curve by reducing strength of source term by a factor of 2 to account for the uncertainty of source estimation. At 100 keV and 500 keV hiss diffusion curve agrees well with measured electron distribution in terms of shape. The agreement at 1 MeV is worse but it does not exclude the possibility that hiss along with other loss mechanisms precipitate electrons.

This case from Figure 4.3 is the best among all 38 cases in terms of shape match between measurements and theory for electrons at 100 and 500 keV. No chorus or EMIC wave was

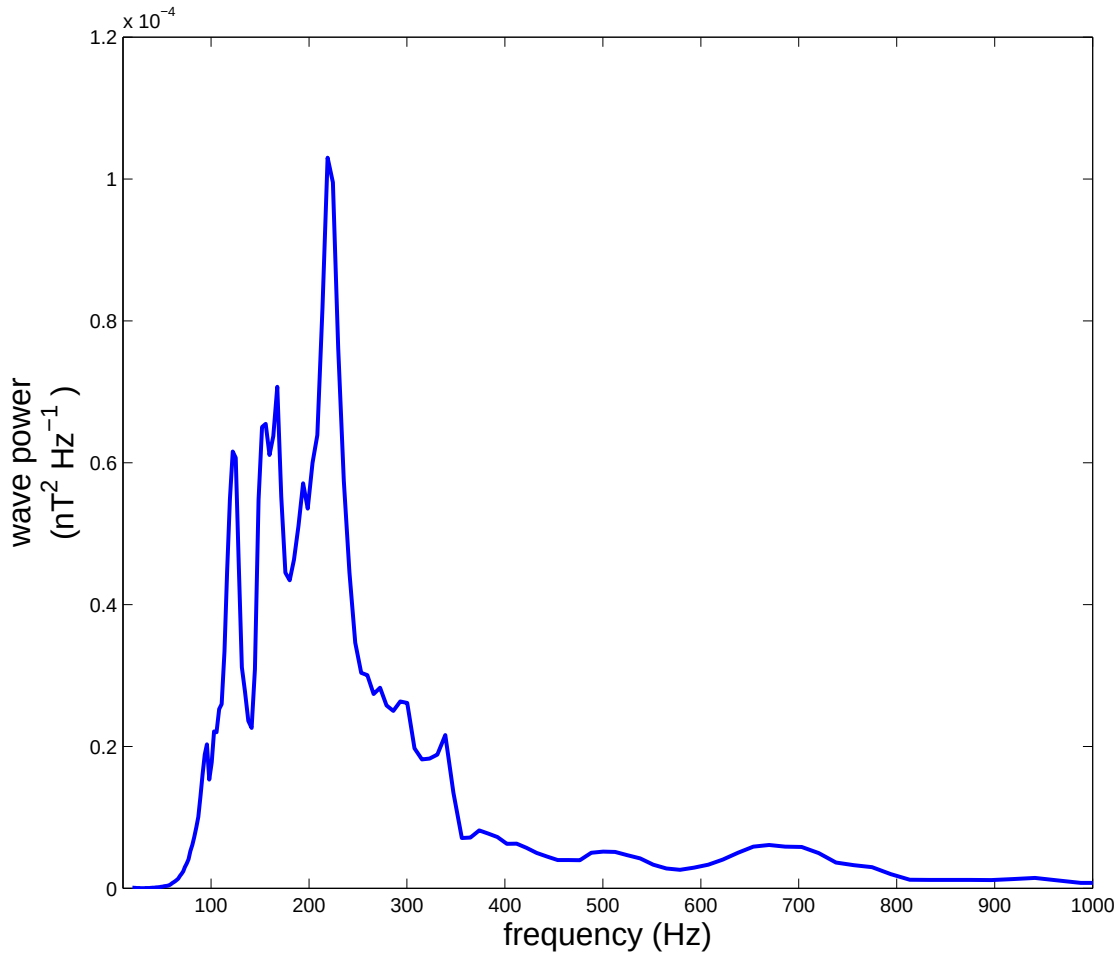

Figure 4.2: Hiss wave power spectra at 21:15:00-21:15:54, Oct 8, 1991 when UARS and CRRES are at magnetic conjunction

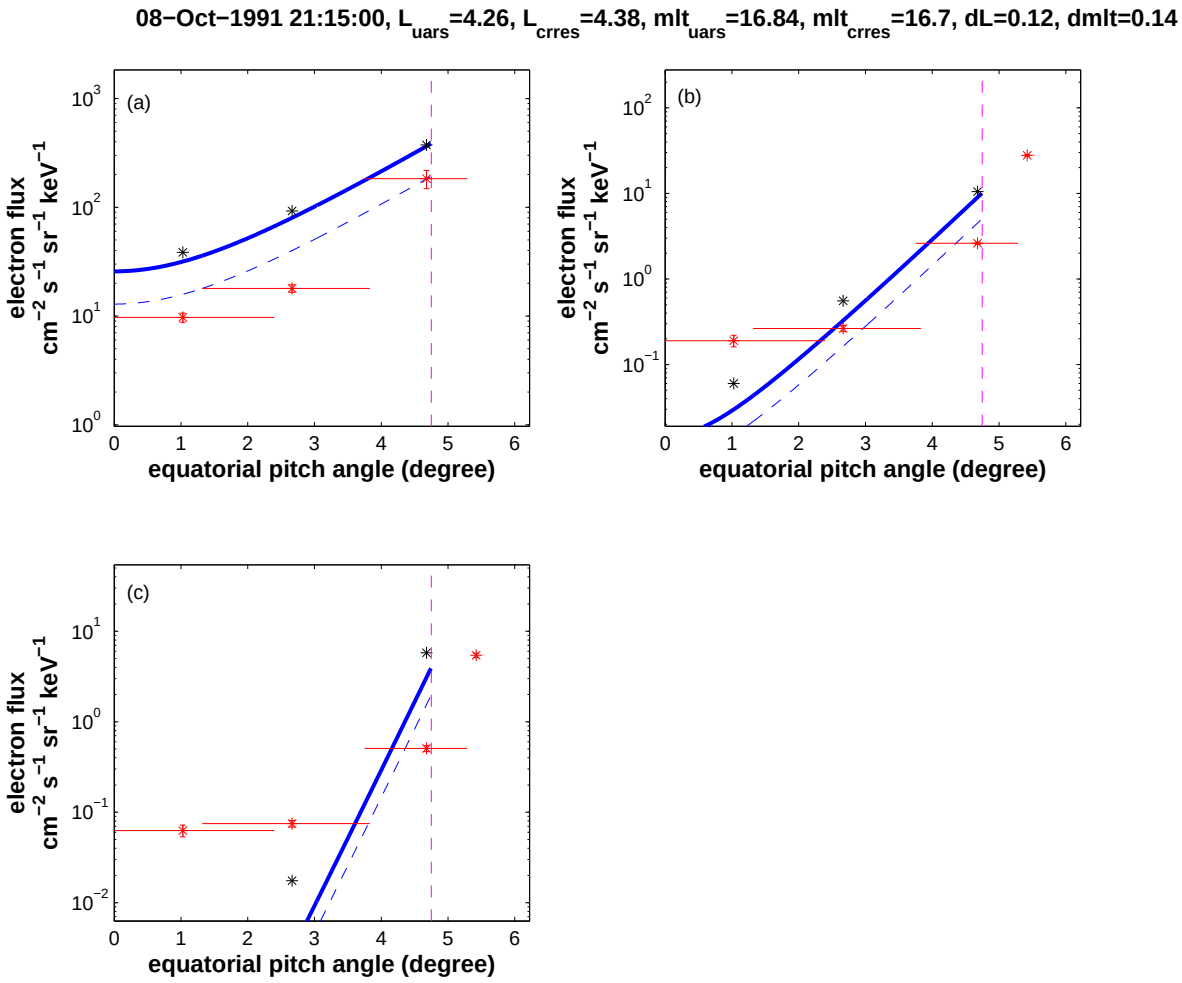

Figure 4.3: Comparison of hiss diffusion curve to measured electron flux at loss cone. he vertical magenta dash line plots edge of bounce loss cone. **(a)** 100 keV electron flux vs hiss diffusion, the red stars are measured electron flux from three electron telescopes inside loss cone , the horizontal color bars are field of view of each telescope, the thick blue curve is electron flux distribution predicted by hiss diffusion, the black stars are integral of blue curve over field of view of each telescope, the dash blue curve is obtained by reducing source term by a factor of 2. **(b)** similar to panel (a) for 500 keV electrons. **(c)** similar to panel (a), for 1MeV electrons

observed at this conjunction which reduces the possibility of other wave modes. Another conjunction between UARS and CRRES occurs at universal time 11:38:01 - 11:38:34 the same day at slot region. The diffusion coefficient at 100 keV given by theory is zero. An empty loss cone is observed. At 500 keV and 1MeV the diffusion coefficients are at small values $10^{-6} - 10^{-7} s^{-1}$. The trapped electron flux is lower than detector sensitivity. There is no electrons available to be scattered. This case is also considered as being consistent with hiss diffusion theory.

4.2 Electron precipitation events inconsistent with hiss diffusion

Most of the time hiss diffusion seems to be far from adequate to account for the amount of precipitation observed. Figure 4.4 shows the observed electron flux at three energy bins versus modified hiss diffusion curve at universal time 00:14:50-00:15:50, Oct 5, 1991. The wave amplitude is about 13 pT. The hiss diffusion coefficients are magnified by a factor of 10,000 at 100 keV, and 2000 at 500 keV and 1MeV to match the measurements. The hiss diffusion is negligible compared to the large amount of precipitating electrons observed. There is no chorus or EMIC wave present at this conjunction. Among 38 cases there are 25 cases resembling this one with two cases coinciding with EMIC waves and 4 coinciding with chorus waves.

Figure 4.5 gives another type of electron precipitation that can not be explained by hiss diffusion. The flat isotropic distribution across loss cone is either from strong diffusion or non-diffusive mechanism. The hiss diffusion is too small to cause strong diffusion as indicated by the steep diffusion curve.

Sometimes the electron distribution is step-like with a flux drop at the edge of loss cone and flat inside loss cone. One example is given by Figure 4.6. This electron profile does not look like from a diffusion process. Some non-diffusive process like atmospheric backscattering is a possible mechanism.

There is only one case that hiss diffusion theory seems to overestimate the amount of precipitating electrons given as shown in panel (a) of Figure 4.7. It is at universal time

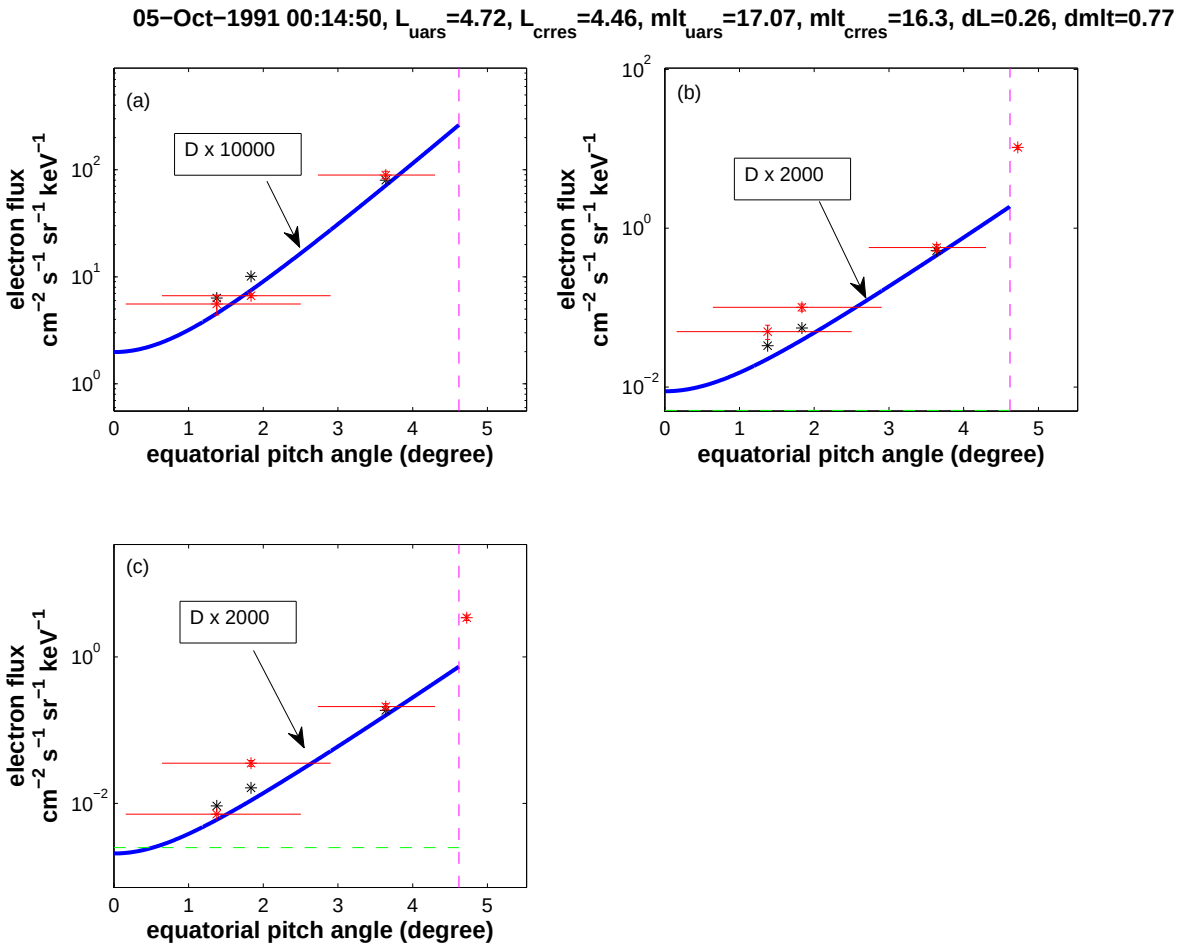

Figure 4.4: Comparison of modified hiss diffusion curve to measured electron flux at loss cone. The vertical magenta dash line plots edge of bounce loss cone whereas the horizontal green dash line is detector sensitivity.**(a)** 100 keV electron flux vs hiss diffusion, the red stars are measured electron flux from three electron telescopes inside loss cone , the horizontal color bars are field of view of each telescope, the thick blue curve is electron flux distribution predicted by hiss diffusion with diffusion coefficient increased by a factor of 10,000, the black stars are integral of blue curve over field of view of each telescope. **(b)** similar to panel (a) for 500 keV electrons with diffusion coefficient boosted up by a factor of 2000. **(c)** similar to panel (a), for 1MeV electrons with diffusion coefficient boosted up by a factor of 2000

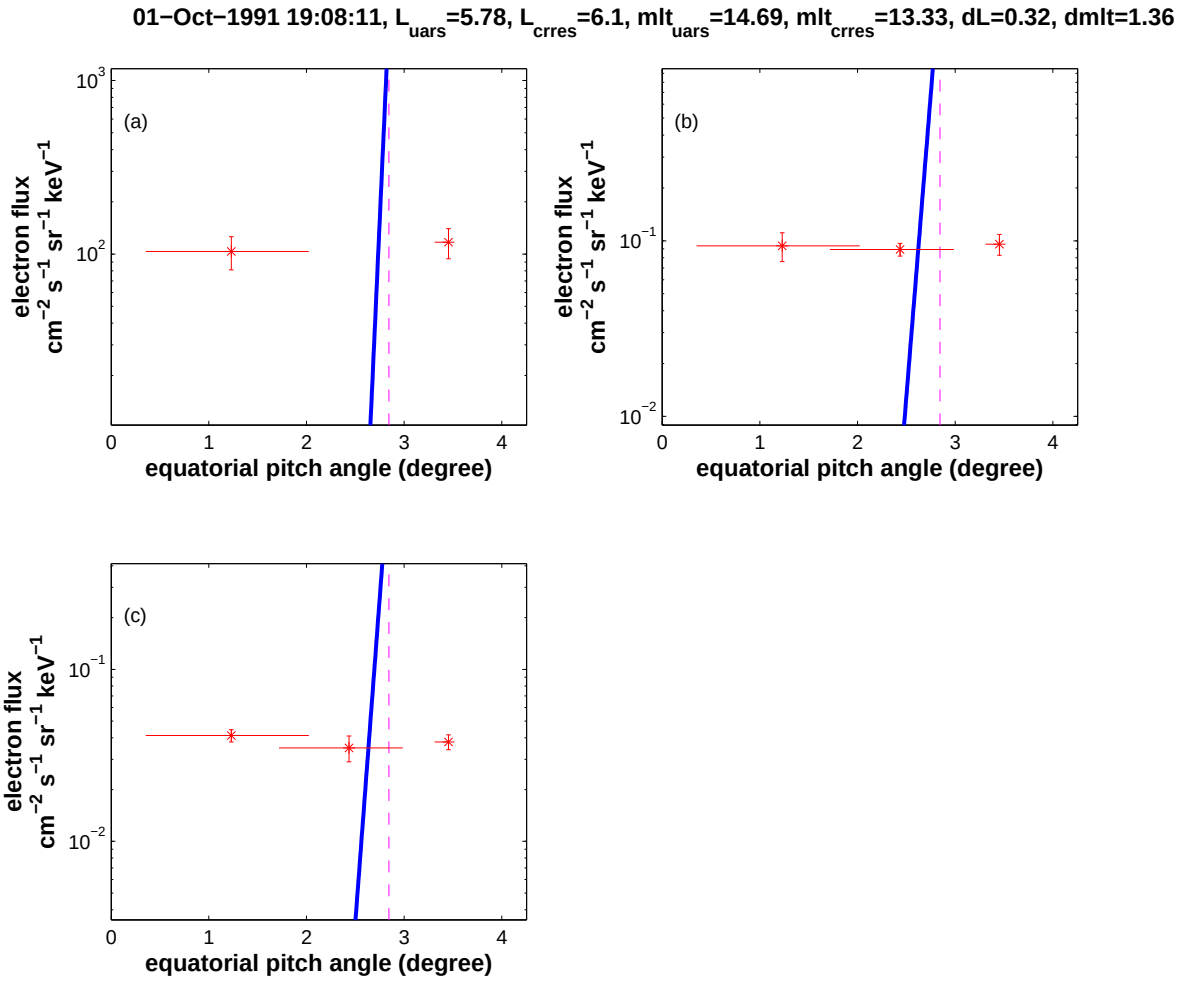

Figure 4.5: Comparison of hiss diffusion curve to measured electron flux at loss cone. The vertical magenta dash line plots edge of bounce loss cone. **(a)** 100 keV electron flux vs hiss diffusion, the red stars are measured electron flux from three electron telescopes inside loss cone , the horizontal color bars are field of view of each telescope, the thick blue curve is electron flux distribution predicted by hiss diffusion. **(b)** similar to panel (a) for 500 keV electrons **(c)** similar to panel (a), for 1MeV electrons

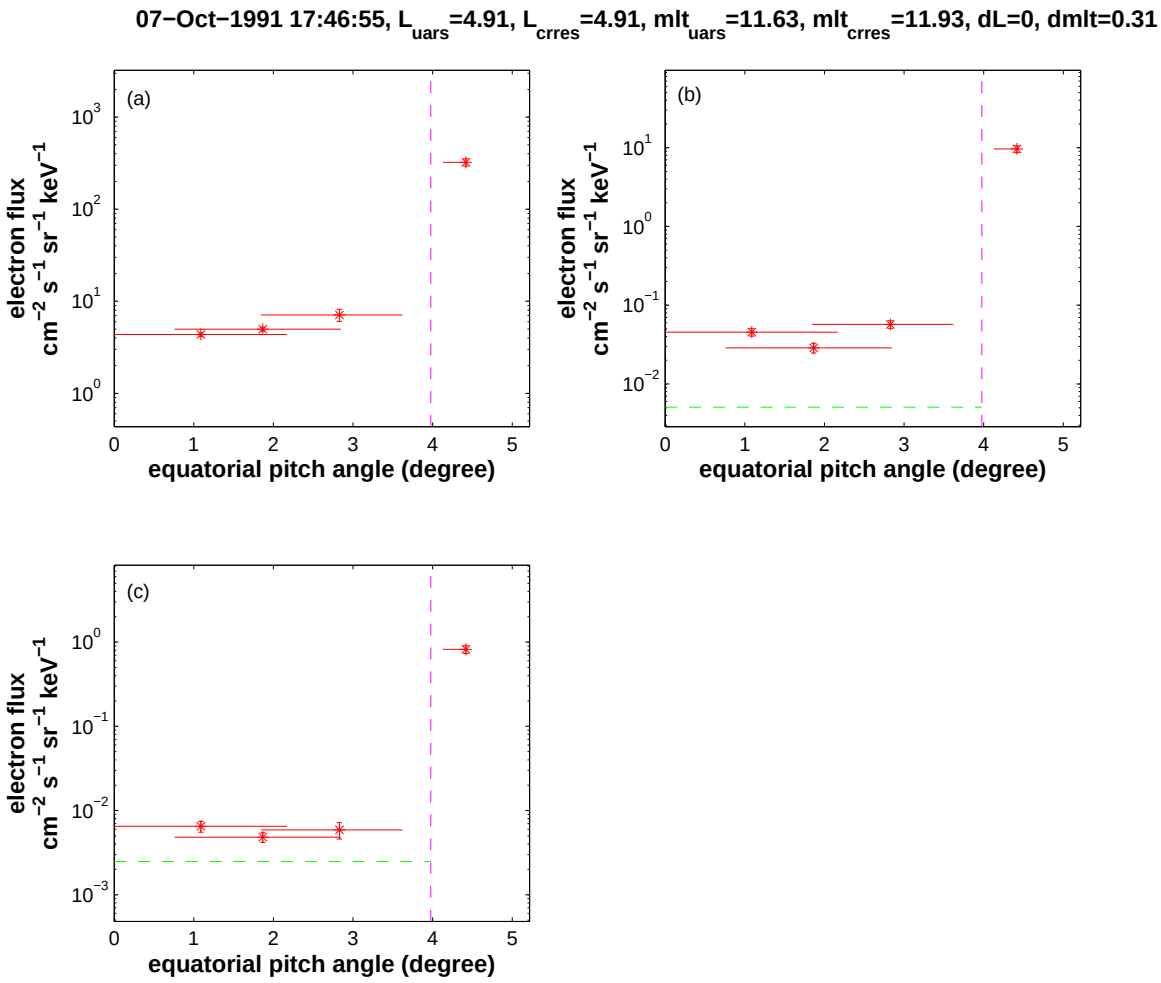

Figure 4.6: Electron flux pitch angle profile with sharp edge of loss cone and flat distribution inside loss cone. The vertical magenta dash line plots edge of bounce loss cone. The horizontal green dash line is detector sensitivity

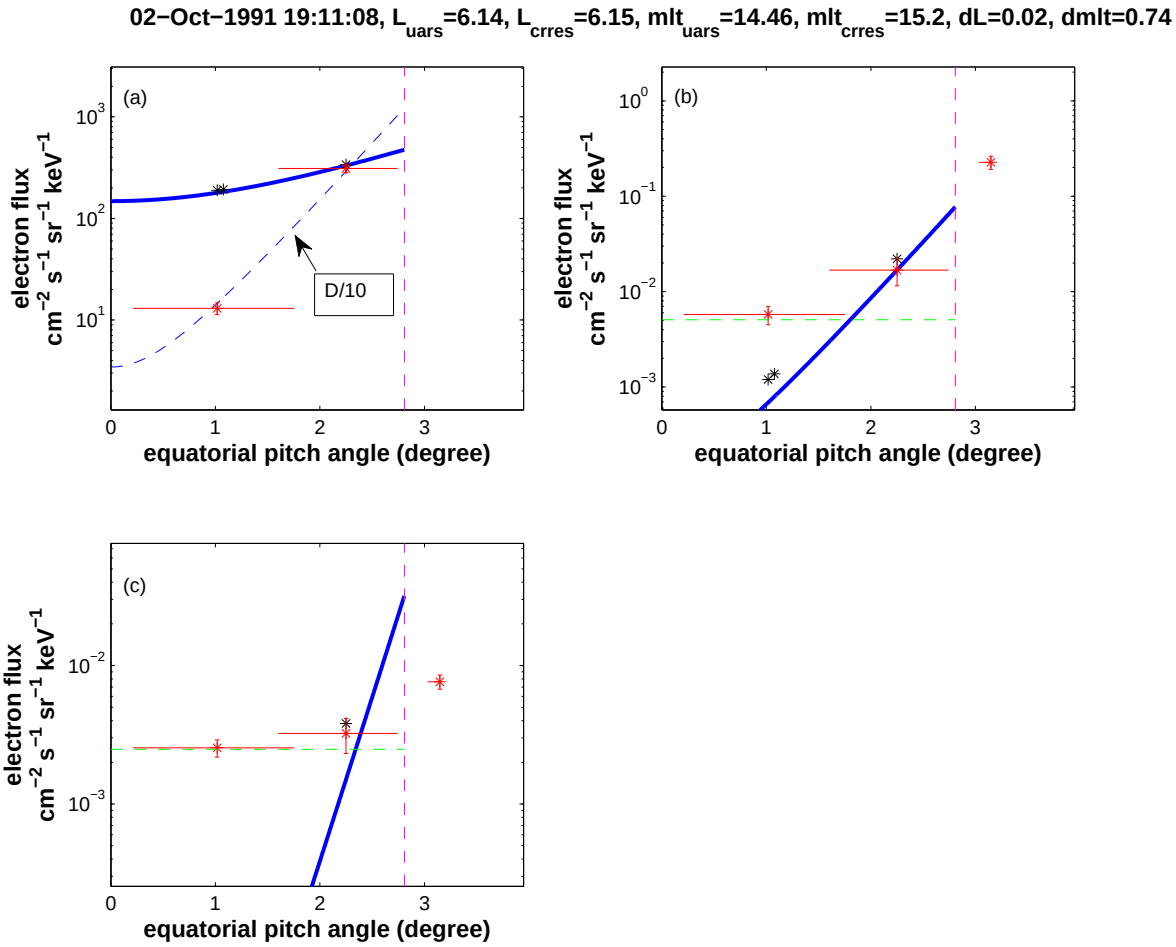

Figure 4.7: Comparison of hiss diffusion curve to measured electron flux at loss cone. The the vertical magenta dash line plots edge of bounce loss cone. The horizontal green dash line is detector sensitivity. **(a)** 100 keV electron flux vs hiss diffusion, the red stars are measured electron flux from three electron telescopes inside loss cone , the horizontal color bars are field of view of each telescope, the thick blue curve is electron flux distribution predicted by hiss diffusion, the dash blue line is hiss curve with diffusion coefficient decreased by a factor of 10, **(b)** similar to panel (a) for 500 keV electrons **(c)** similar to panel (a), for 1MeV electrons

19:11:08 - 19:12:20, Oct 2 , 1991. The amplitude of hiss is about 62pT. The diffusion coefficient at 100 keV has to go down by a factor of 10 to fit the observation. As mentioned earlier, the choice of wave normal angle model does not make big difference. There is no knob to be tuned in the model to fit the measured electron flux. The UARS electron correction algorithm at this event is less reliable at 100 keV due to proton over correction. It is unclear if the discrepancy is caused by assumptions in the diffusion model or electron data correction algorithm.

4.3 Conclusion for hiss diffusion theory testing

As mentioned in Chapter 2 there was a magnetic storm with minimum Dst -149 nT in the first ten days of October 1991. The 38 magnetic conjunctions between UARS and CRRES spread out over all phases of the magnetic storm. Hiss has been proposed to be the main loss mechanism during quiet time [31, 48]. Thus the storm time cases might not be ideal for testing the theory of electron precipitation by hiss diffusion. There are two cases showing good consistency between hiss theory and measured electron loss cone distribution. In only one case hiss predicts more electrons than observed at 100 keV due to some unknown factor either from theory or data correction algorithm. Most of the time hiss diffusion is far from sufficient to account for the large amount of precipitation observed which suggests existence of other unknown mechanisms. There is no case that the presence of hiss causes no electron precipitation. Therefore, it is concluded that the hiss diffusion theory seems be consistent with the electron loss cone distribution when no other loss mechanism is present.

Chapter 5

COMPARISON OF EMIC WAVE DIFFUSION TO PRECIPITATING AND TRAPPED ELECTRONS BOTH AT LOW EARTH ORBIT AND MAGNETIC EQUATOR

As mentioned in the first chapter, quasi-linear theory of EMIC wave scattering predicts strong diffusion at loss cone, fast depletion of trapped electrons, pancake-shape distribution of trapped electrons resulting from selective scattering at low and medium pitch angles, and relativistic electron precipitation embedded in broader precipitation of tens of keV ions. In the following sections, the measured loss cone distribution will be compared to what the quasi-linear theory predicts. The trapped electron profile and selective pitch angle scattering will be examined as well. At the end the findings will be compared to those from other authors to have a better understanding of current quasi-linear theory of EMIC diffusion and the role of EMIC waves in radiation belt electron loss.

5.1 Case studies

5.1.1 Testing the theory with electrons at loss cone

Among about 38 magnetic conjunctions between UARS and CRRES during the first ten days of October 1991, only three coincide with EMIC wave activities at the vicinity of magnetic equator. Right column of Figure 5.1 show three groups EMIC waves (labeled as case 1, 2 and 3) observed by CRRES satellite at north of magnetic equator with latitude within about 8°. All three EMIC wave events are characterized as peaking at hydrogen band and being left hand polarized most of the time according to comprehensive list of EMIC waves by Emeritus Prof Brian Fraser from University of Newcastle. The EMIC waves are spotted with a combination of manual checking on the wave power near ion cyclotron frequencies,

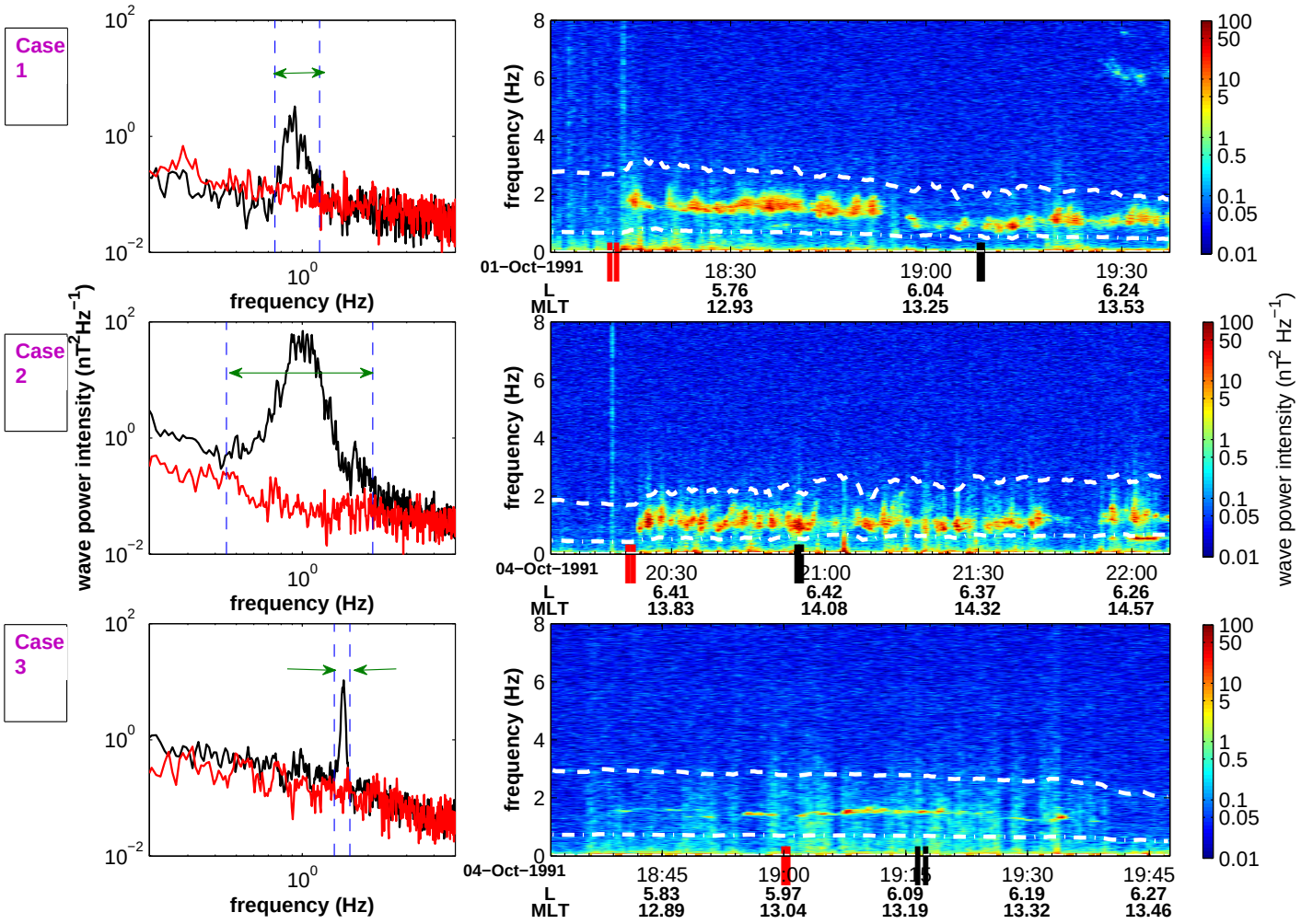

Figure 5.1: Three EMIC wave events from CRRES with case 1 on October 1st, 1991 and case 2 and 3 at two consecutive orbits on Oct 4th, 1991. The right column panels plot wave power spectrum on frequency domain versus universal time, L shell and magnetic local time. The black double lines on UT axis marks the time slots when UARS is at footprint of CRRES (aka conjunction). The red double line marks the reference time. Two white dash lines from top to bottom within each panel are local hydrogen and helium gyro-frequencies. The left column panels plot wave power spectrum at the time slots marked the double black and red lines in the right column. The black curve is wave power spectrum at the conjunction time while red curve is wave power at reference time. The blue vertical dash lines show cutoff frequencies bounding the peaks.

wave power above the instrument noise level of about $10^{-3} nT^2/Hz$ and polarization analysis carried by Prof Brian Fraser.

The black curves in the left column of Figure 5.1 are wave power spectrum on frequency domain at the conjunction time intervals marked by the double black lines in the right column. The red curves are the 'background' wave power spectrum at reference when there is no EMIC wave marked by the red double lines in the right column. The EMIC wave power spectrum is obtained by subtracting red curve from black curve. The two blue vertical dash lines are cutoff frequencies picked manually. It is assumed that wave power is zero outside the frequency range bounded by cutoff frequencies. Then the wave power spectrum along with L shell , cold plasma density and electron energy are fed to the diffusion coefficients formula given in Chapter 3 to compute diffusion coefficients. It is assumed that EMIC waves are confined within 8° latitude of magnetic equator. The diffusion coefficient will be larger with larger latitude range. Only diffusion at hydrogen band is computed. Two Gaussian wave normal angle models are used: parallel propagating and oblique at 30°. The Gaussian width for both models is 15°. The minimum resonant energy is computed as well to have independent check on the diffusion coefficient formula. The minimum energy is determined by using equations (3),(4) and (5) in Denton et al 2015 [11]. Denton's formulas are based on first order resonance condition and EMIC wave dispersion relationship.

The electron flux from UARS at conjunctions are plotted in the top three rows of Figure 5.2. The left, middle and three columns correspond to case 1, 2, and 3 respectively. The red dots are electron flux observed right outside loss cone. Blue, green and cyan are for electrons inside loss cone. The closeness of conjunctions in terms of McIlain L shell and magnetic local time is plotted in Row (d). The bottom row plots L shell profile of both trapped (red) and precipitating(blue, green and cyan) 1MeV electron flux at a time window of one minute right before and after conjunctions. The center location of conjunctions is marked by the vertical dash lines.

For the first conjunction at universal time 19:08:11 to 19:08:40 on Oct 1st, 1991, isotropic distribution across loss cone is observed. The peak EMIC wave power is about 3.28 $nT^2 Hz^{-1}$

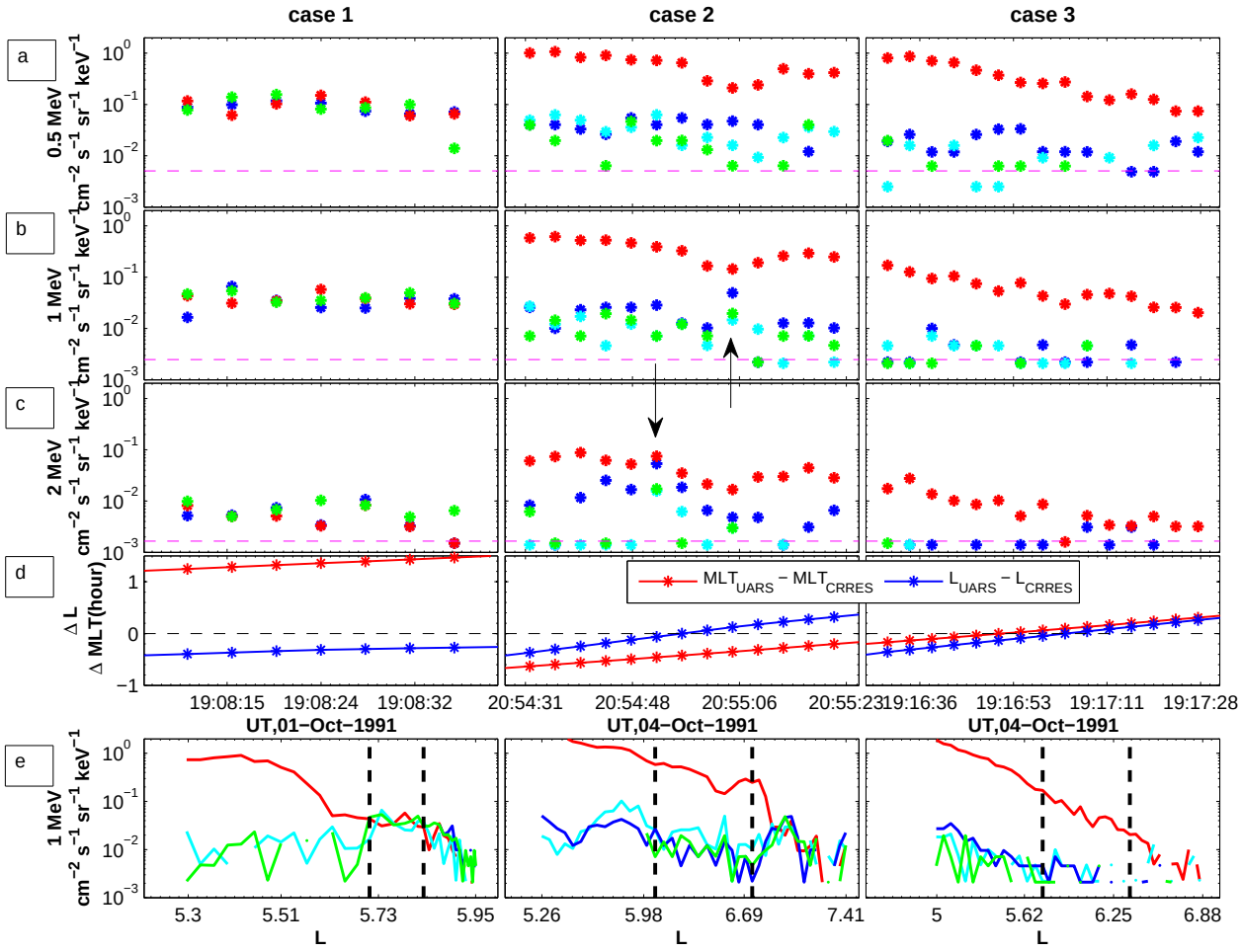

Figure 5.2: Trapped and precipitating electron flux observed by UARS at three UARS/CRRES conjunctions. The left,middle and right columns correspond to case 1,2, and 3 respectively. From top to bottom, **(a)** 0.5 MeV electron differential flux with red for electron telescope right outside loss cone , blue, green and cyan for three telescopes well inside loss cone, the horizontal magenta dash lines show detector sensitivity, those below sensitivity line are due to over-correction of correction algorithm, **(b)** and **(c)**1MeV and 2MeV electron differential flux with color code the same as 0.5 MeV electrons. The events pointed by the two black arrows are re-plotted in Figure 5.3 and 5.4. **(d)** difference of L shell and magnetic local time of UARS (magenta) and CRRES(blue),**(e)** L profile of 1MeV electron flux at time window of one minute right before and after conjunction, red for electron telescope right outside loss cone, blue, green and cyan for three telescopes well inside loss cone. The vertical two black dash lines bound the conjunction window.

at 0.925 Hz. The cold plasma density is 7.23 cm^{-3}. The cutoff frequencies are 0.75 Hz at lower end and 1.2 Hz at higher end. The local proton gyro-frequency is 2.23 Hz. The minimum resonant energy given by Denton's formula at 1.2 Hz is about 8.35 MeV. The diffusion coefficients are all zeros at 0.5, 1 and 2 MeV. The isotropic distribution looks like to be the signature of strong diffusion from EMIC wave as predicted by the theory. However, the zero diffusion coefficients and high minimum resonant energy excludes this possibility. Furthermore, the isotropic distribution is spotted twice again without presence of EMIC waves at UT 20:44:51 and 22:22:16 when UARS traverses the same L and approximately same magnetic local time. Since early 1970s, it has been known that isotropic distribution is very commonly found at trapping boundary of radiation belts where the particle gyro-radius is comparable to the curvature of Earth's magnetic field [16]. By looking at wider time window of one minute right before and after conjunction (bottom row of Figure 5.2), it is clear that case 1 conjunction occurs right at some boundary while case 2 and 3 are not. Trapping boundary is a spatial structure that can be seen quite often by multiple passes of low Earth orbit satellites regardless of presence of EMIC waves. More details about properties of trapping boundaries can be found in Imhof's investigation on UARS data in 1997[17]. Therefore it is likely that the isotropic distribution here is because UARS is at trapping boundary. That EMIC wave and strong precipitation appear at the same time doesn't mean the two should have connection. This case demonstrates the importance of quantitative evaluation in linking EMIC wave to electron precipitation.

The second conjunction occurs around 20:55, Oct 4th, 1991. The electron precipitation is embedded in a broad ion precipitation. Figure 5.5 show such enhancement of tens of keV proton precipitation at a time window that well encapsulates the time frame of electron precipitation at 20:54:30 - 20:55:20. The flux of precipitating protons at 74 -80 keV is greater than 10^3 $cm^{-2}s^{-1}sr^{-1}keV^{-1}$. Though measurement of trapped protons is not available, from POES observed EMIC wave- driven proton precipitation at about same location (see Engebretson et al in 2015 [12]), this amount of precipitating proton flux is comparable to typical flux of trapped protons. This is a signature of EMIC wave scattering protons. The

EMIC wave is more intense than that in the first case peaking 69.68 nT^2Hz^{-1} at 1.005 Hz. The cold plasma density is 11.36 cm^{-3}. The cutoff frequencies are 0.45 at lower end and 2.1 Hz at higher end. The local proton gyro-frequency is 2.13 Hz. The minimum resonant energy is 139 keV. The loss cone diffusion coefficients from parallel propagating wave model are 0.0107 s^{-1} at 0.5 MeV, 0.0151 s^{-1} at 1 MeV and 0.0298 s^{-1} at 2MeV. Oblique wave model gives 0.0070 s^{-1} at 0.5 MeV, 0.0199 s^{-1} at 1 MeV and 0.0176 s^{-1} at 2 MeV. Either model suggests diffusion hits the strong diffusion limit of 0.0066 s^{-1} at 0.5 MeV , 0.0073 s^{-1} at 1 MeV and 0.0075 s^{-1} at 2 MeV. Thus an isotropic distribution across loss cone is expected. Contrarily, the measured trapped flux is one to two order of magnitude higher than flux inside loss cone as shown in the middle panels of Row (a)-(c) in Figure 5.2. The closest point between trapped and precipitating flux occurs at 20:54:52 and 20:55:05 UT (pointed by the arrows). The electron flux at these two time stamps is re-plotted in Figure 5.3 and 5.4 over pitch angle space for comparison to the theoretical EMIC wave diffusion curves. As mentioned in Chapter 3, the theoretical curves are forced to line up with electron flux right outside loss cone. Even at the nearest point, the discrepancy between observation and theory is still very large. The diffusion coefficients given by parallel model have to go down by a factor of about 16 for 1MeV electrons and 13 for 2 MeV electrons to fit the observation. The diffusion coefficients given by oblique model need to be decreased by a factor of 21 at 1 MeV and 9 at 2 MeV. It seems that the discrepancy shrinks from 1 MeV to 2 MeV.

In case 2 since the higher end cutoff frequency is close to the proton gyro-frequency, small change of the cutoff frequency will change the minimum resonant energy by noticeable amount. If the cutoff is chosen to be at 1.665 Hz as shown in Figure 5.6, the minimum resonant energy jumps to 1.75 MeV. The diffusion coefficients at 0.5 and 1 MeV go to zero. Then the 1 MeV electron precipitation at 21:55:05 UT can not be explained by EMIC wave diffusion. But the diffusion coefficient of 2 MeV is 0.0154 s^{-1} which still goes beyond strong diffusion limit. The large discrepancy between the theory and observation still exists.

The third conjunction case occurs around 19:17 Oct 4th, 1991. The peak EMIC wave power is about 20.93 nT^2Hz^{-1} at 1.55 Hz.The cold plasma density is 9.73 cm^{-3}. The cutoff

frequencies are 1.4 Hz at lower end and 1.65 Hz and higher end. The local proton gyrofrequency is 2.77 Hz. The diffusion coefficients from both parallel and oblique models are zero at 0.5, 1 and 2 MeV. The minimum resonant energy is 6.3 MeV. The non-empty loss cone might be filled by other processes if the theory gives the correct amount of diffusion.

5.1.2 Testing the theory with profile of trapped electrons

The second EMIC wave event lasts for about two hours with a 12min gap between 21:42 and 21:54. The CRRES spacecraft is moving very slow and mostly azimuthally. It stays at the same L shell of about 6.4 and spans only 0.65 hr in magnetic local time from 20:23 to 21:42 UT, which suggests the electron flux variation observed by CRRES is mostly temporal variation. It is good opportunity to test what has been suggested by Summers [46] that EMIC wave residing in just 1 percent of magnetic local time is able to empty the radiation belt at a time scale of a couple of hours.

The time evolution of electron flux from CRRES MEA is compared to EMIC wave diffusion curve. In short time period, the characteristic decay time of EMIC waves at small pitch angle is reciprocal of bounce averaged diffusion coefficient[30]. In a time period much longer than drift period, the magnetic local time distribution of EMIC waves need to be considered to compute bounce-drift averaged diffusion. It is assumed that EMIC wave is confined within 0.65 hr of magnetic local time as from the observation. The EMIC wave diffusion curves for both bounce and bounce-drift averaged diffusion are plotted in the middle row of Figure 5.7. The thin solid and dash red lines are bounce-drift averaged and bounce-averaged diffusion respectively. The thick wiggly blue curve is electron flux at pitch angle of 5° measured by MEA electron telescope on board CRRES at 1090 keV. Obviously the measured electron profile matches neither bounce-drift averaged nor bounce-averaged diffusion.

At the vicinity of wave onset the 1090 keV electron flux drops by about a factor of 2 at all pitch angles as shown in the top row of Figure 5.7. There seems to be a connection between electron flux drop and EMIC wave. However the flux drop seems to begin at 20:22 one minute before the wave onset and occurs at all pitch angles. EMIC wave diffusion theory

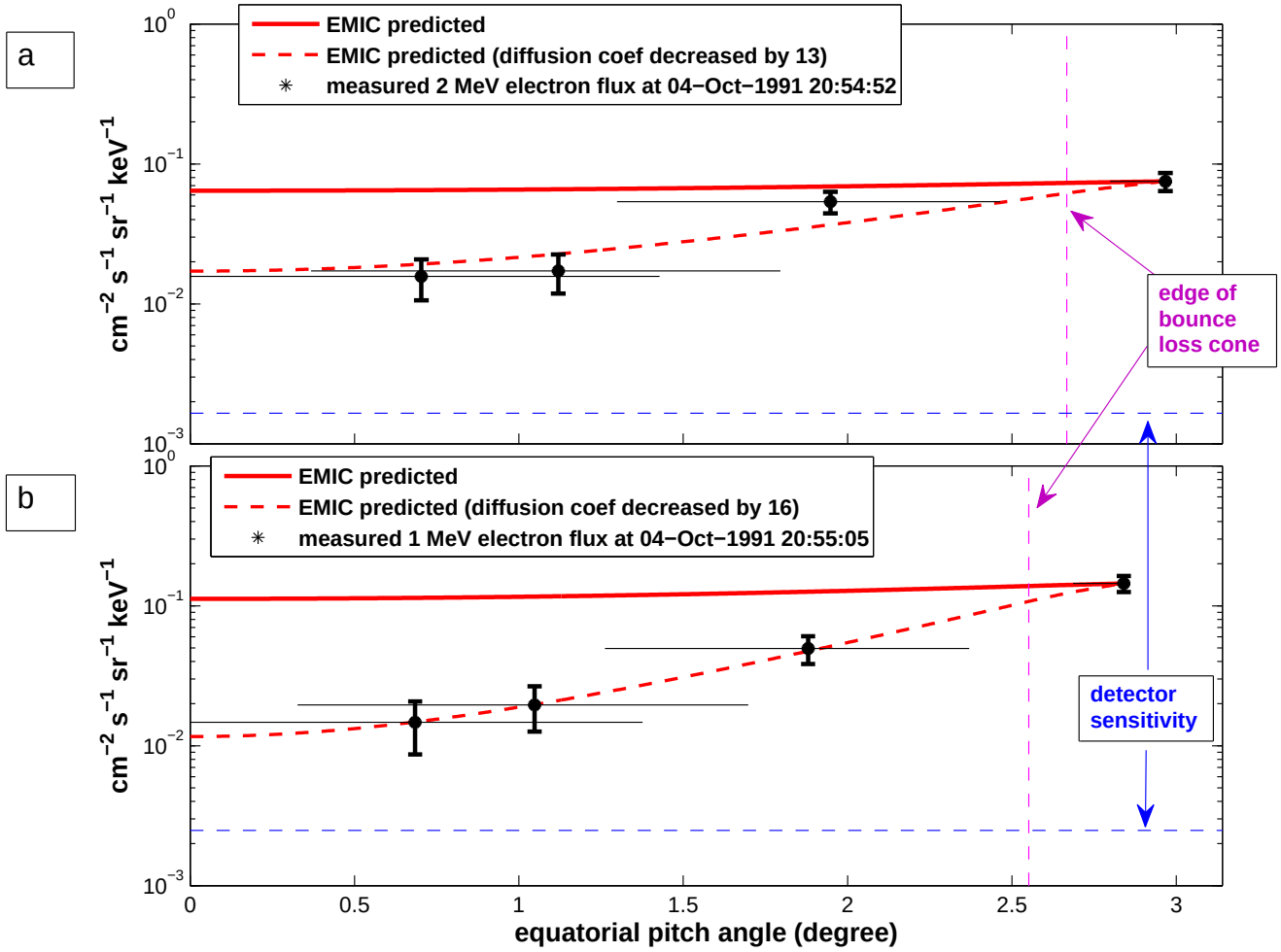

Figure 5.3: Comparison of theoretical loss cone distribution to measurements from UARS around 21:55 UT, Oct 4, 1991. The diffusion coefficients are computed assuming parallel propagating EMIC waves. Row (a) and (b) are for 2MeV and 1MeV electrons respectively. The red thick curves are prediction given by EMIC wave diffusion theory. Red dash lines are EMIC wave curve with diffusion coefficients decreased by a factor of 16 for 1MeV electrons and 13 for 2 MeV electrons. The black dots are electron differential flux measured by four telescopes on board UARS with one right outside loss cone, three inside loss cone. The horizontal error bars are field of view of telescopes. The pink vertical dash lines mark the edge of bounce loss cone. The detector sensitivity is marked by horizontal blue dash lines. The pitch angles of UARS telescopes at low Earth orbit are converted into equatorial values in degree.

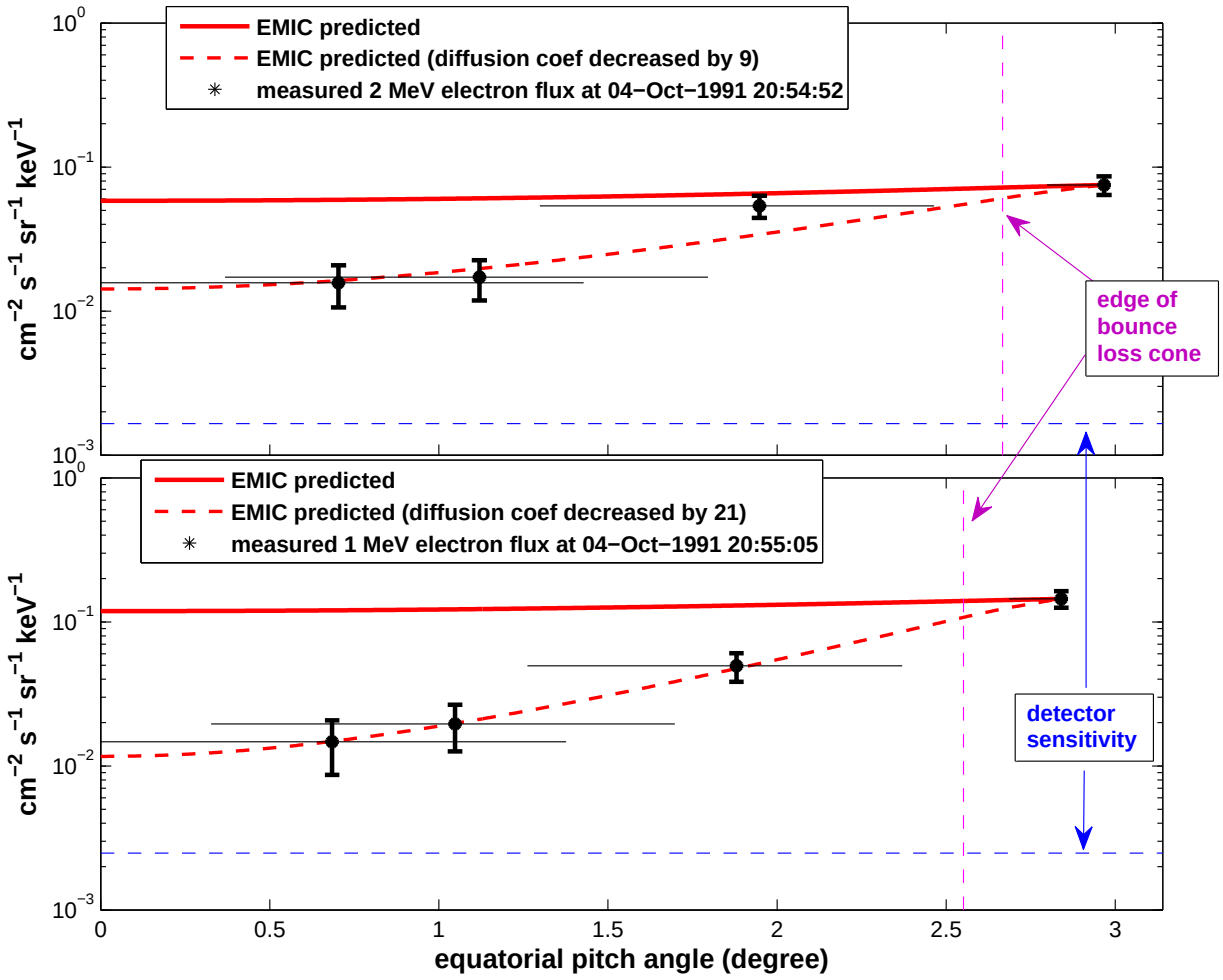

Figure 5.4: Similar to Figure 5.3, assuming oblique propagating EMIC waves

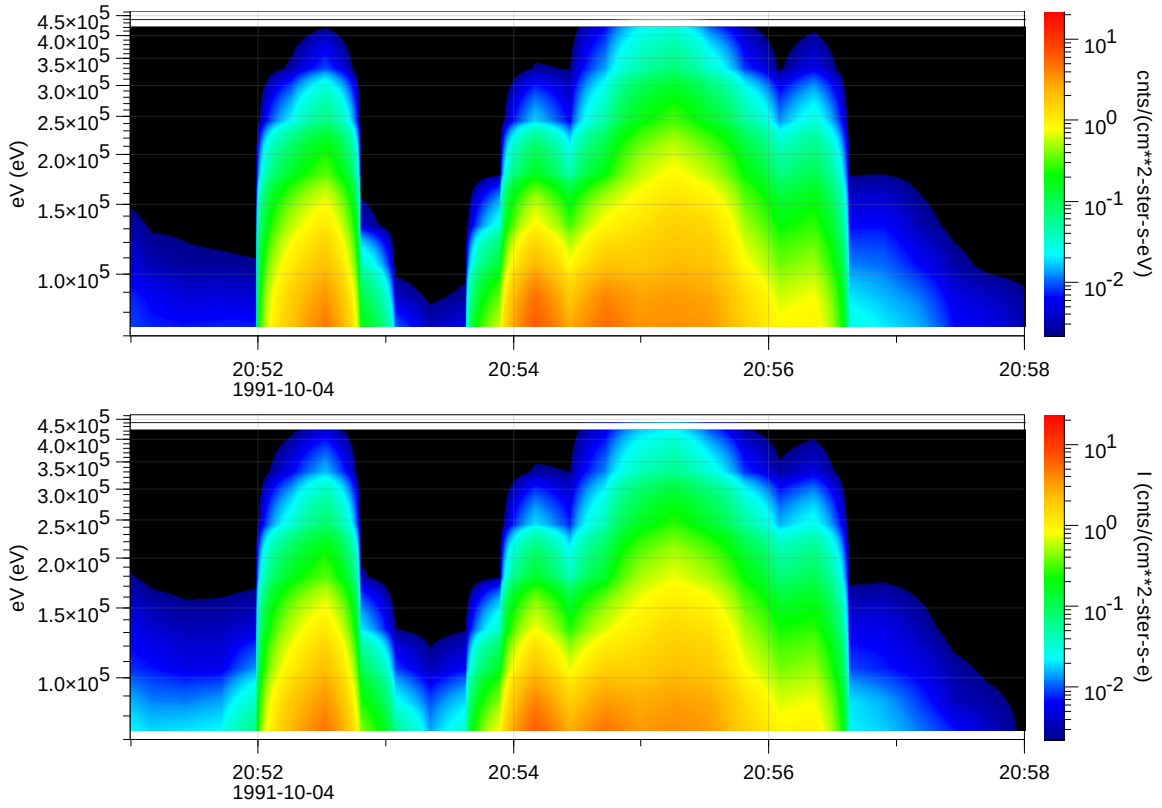

Figure 5.5: Precipitating protons from UARS at 550km. The upper and bottom panels plot proton flux at pitch angle 22° and 14° respectively. Both are well inside bounce loss cone. The UARS /CRRES conjunction is at 20:54:30 to 20:55:20 well inside the proton precipitation window. The lower energy cutoff is 74 keV. Notice that the energy is in eV and flux is in $cm^{-2}s^{-1}sr^{-1}eV^{-1}$.

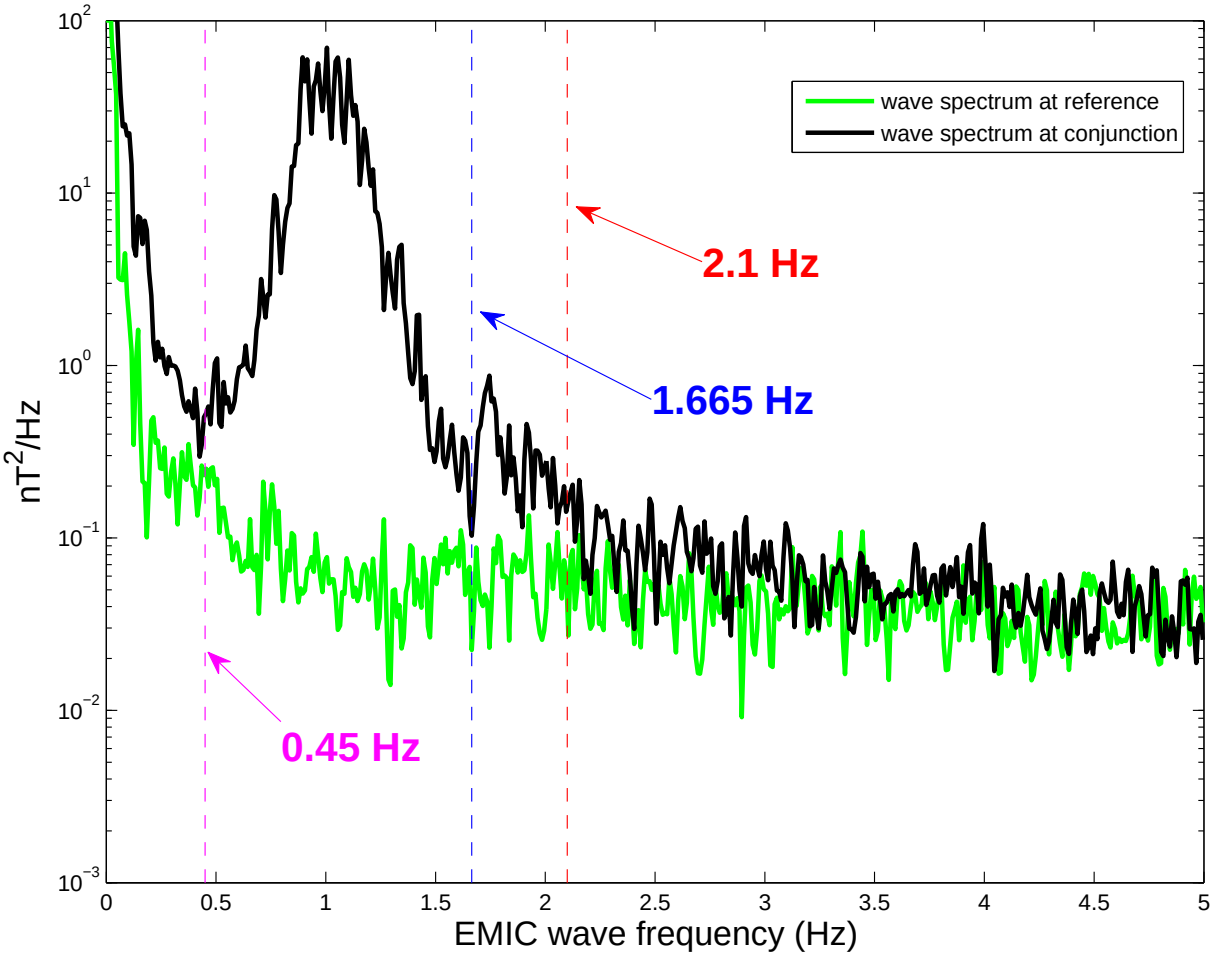

Figure 5.6: Two choices of cutoff frequencies. The black curve is wave power spectrum at case 2 conjunction around 21:55 UT, Oct 4, 1991. The green curve is the wave power spectrum used as background and measured around 20:21 UT, Oct 4, 1991. The magenta vertical dash line marks lower end cutoff frequency of 0.45 Hz, blue and red lines mark two choices of cutoff frequencies of 1.665 Hz and 2.1 Hz at higher end

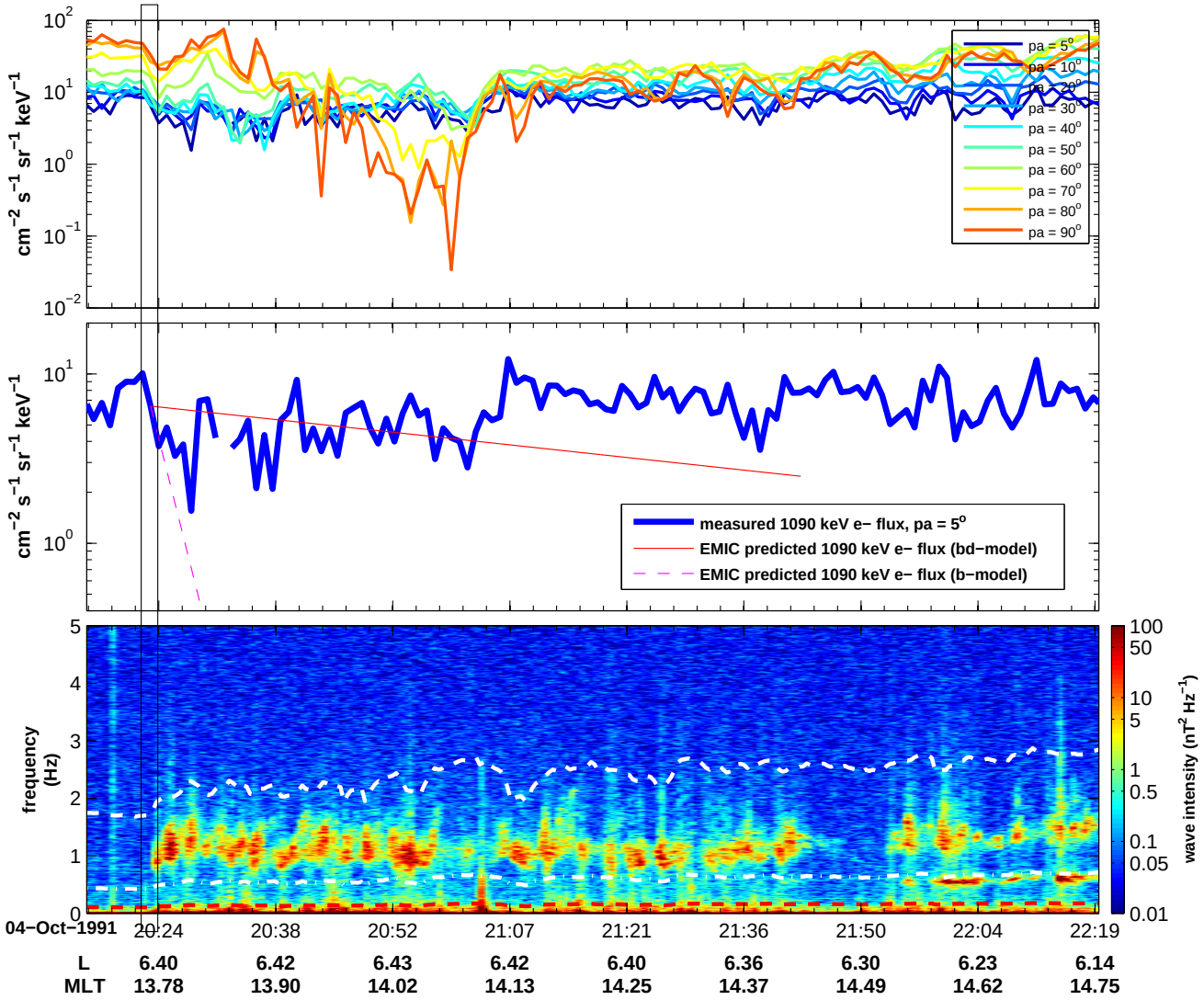

Figure 5.7: Comparison of trapped electron from MEA on board CRRES to EMIC wave diffusion. **(a)** differential flux of 1090 keV electrons at pitch angles from 5° to 90°. **(b)** thick blue curve is 1090 keV electron differential flux at pitch angle of 5° measured by MEA. The thin solid red line is prediction from EMIC wave diffusion with bounce-drift averaged model. The dash magenta line is prediction from EMIC wave diffusion with bounce-averaged model. **(c)**EMIC wave spectrogram versus universal time, L shell and magnetic local time. The two white meandering dash lines from top to bottom mark local hydrogen and helium gyro-frequencies.

suggests the diffusion is effective only at low and medium pitch. Furthermore, multiple such flux pulsation were observed in several hours right before the wave onset. It is unlikely that EMIC wave would cause such flux drop.

A correlation study between square of EMIC wave amplitude and electron flux at small pitch angles (from UT 20:15 to 22:20) is carried out to see if there is any hidden relationship between EMIC wave and electrons at the edge of loss cone (Figure 5.8). The diffusion coefficient is proportional to wave amplitude square. The characteristic decay time is reciprocal of diffusion coefficient for electrons at small pitch angles. As shown in Figure 5.8, the correlation between trapped electron flux outside loss cone and EMIC wave amplitude is very weak. The Pearson correlation coefficients are -0.08 with p-val of 0.2 at 509 keV and -0.12 with p-val of 0.04 at 1090 keV.

Another interesting signature of EMIC wave diffusion is the selective scattering at low and medium pitch angles. Though the electrons near 90° are being peeled off by other processes starting at 20:38 UT which make it more difficult to see selective scattering, there are time intervals without obscuring during the 2-hour long wave activities. No selective scattering is observed.

Before preceding to conclusion, one needs to consider if other processes could mask the EMIC wave scattering from being distinguished. There exist whistler mode electron waves mostly hiss at the same time EMIC wave is observed. The magnitude of diffusion coefficient by hiss scattering is at about $10^{-5}s^{-1}$ three orders of magnitude smaller than EMIC wave diffusion. The electron depletion by EMIC will dominate the loss process according to what the theory predicts. The 1 MeV electron flux at all pitch angles start recovering at 21:00 UT and goes back to about the same level before 20:22 UT and stay relatively constant. If the strong scattering suggested by EMIC wave diffusion theory exists, it would require a very strong local sources to replenish the MeV electrons in a relatively short time.

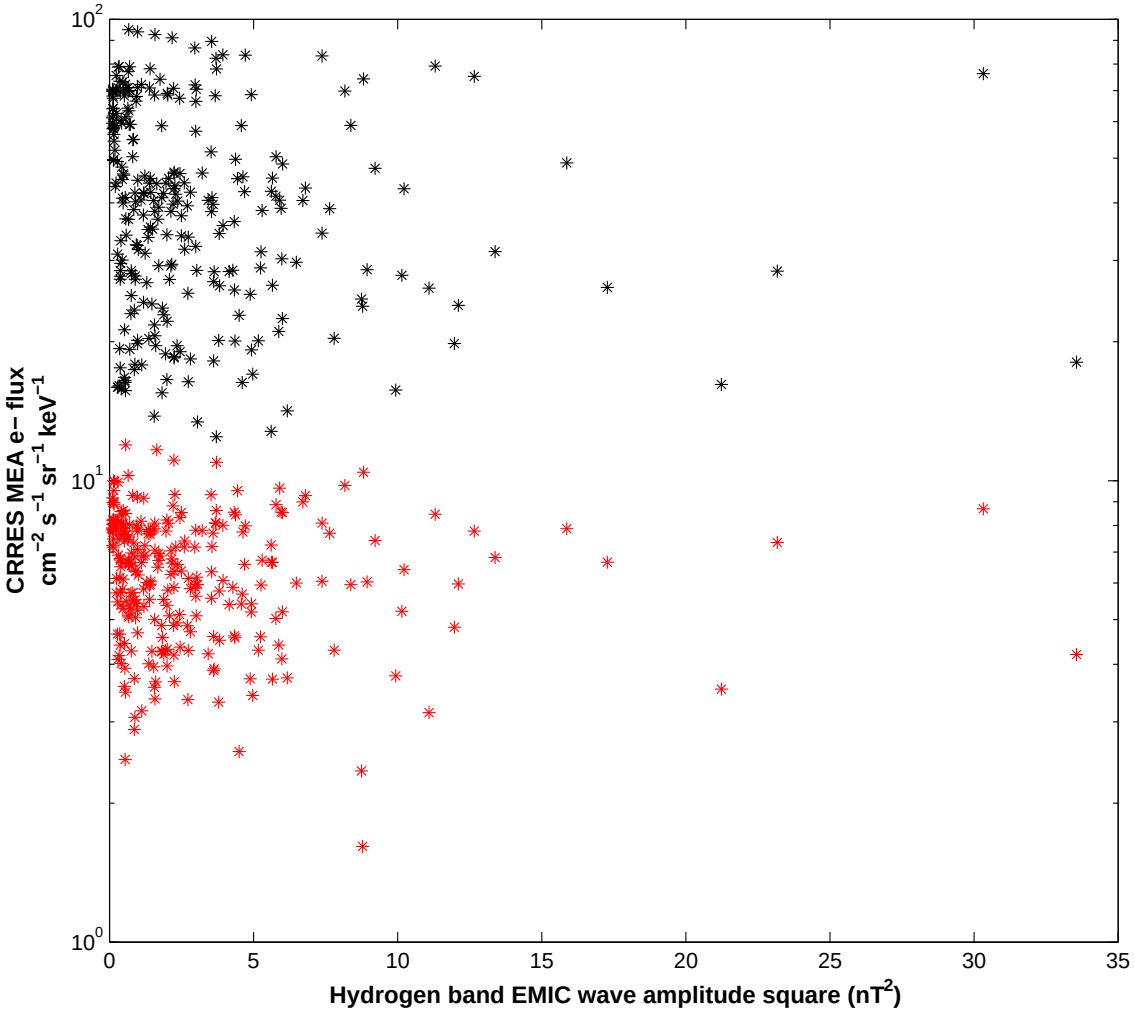

Figure 5.8: hydrogen band EMIC wave amplitude square versus electron flux at pitch angle of 5° measured by MEA on board CRRES. The black and red dots are for 509 keV and 1090 keV respectively.

5.2 Concluding remarks from case studies

To summarize, the electron loss cone distribution deviates largely from what theory predicts. The discrepancy is at least between a factor 9 to 21 depending on the electron energy and wave normal angle models. It seems that the discrepancy at 2 MeV is smaller than at 1 MeV. Neither selective pitch angle scattering nor significant depletion of trapped electrons is observed at energy up to 2 MeV.

5.3 Comparison to findings from others

This section will dive deep into the findings by other authors since 1970s and incorporate findings in this thesis to have a better understanding of EMIC wave diffusion. First of all let us look back to history to see if evidence of strong diffusion (isotropic distribution) at loss cone was reported. Secondly I will relate new findings in this thesis to the seemingly contradictory evidences reported by Rodger and Usanova and Engerbretson. The end of this section will be a discussion of EMIC wave diffusion at ultra-relativistic energy of greater than 2 MeV.

In earlier days when simultaneous wave measurements in magnetosphere was lacking, electron precipitation with simultaneous ion precipitation observed by low Earth orbit satellites were investigated for searching evidence of relativistic electron precipitation by EMIC wave scattering. At the same year Thorne and Kennel [47] first introduced EMIC waves as loss mechanism in 1971, Vampola reported three relativistic events that seemed to be associated with EMIC wave scattering [51]. All three events are just inside plasmapause between late evening and midnight. The isotropy increases toward higher energy. There was no information about wave and protons in Vampola's paper. Later Thorne and Andreoli in 1980 [49] attributed four isotropic electron precipitation events to EMIC wave scattering. Figure 3 of Thorne and Andreoli's paper gives an example of such event. Though simultaneous wave measurement was not available, the broader simultaneous ion precipitation and selective precipitation at higher energy greater than 850 keV look very promising. The

event given by Thorne and Andreoli occurs at a boundary at local time 20.18 hour and L shell of 4.35. This boundary looks very similar to what later study identified as trapping boundary[17]. Isotropic distribution is quite often to be spotted at trapping boundary. By avoiding the trapping boundary events, Imhof in 1986 identified nine energy selective electron precipitation accompanied by ion precipitation near plasmapause at evening local time. The distribution is far from isotropic with electrons near 0° often one order of magnitude lower than electrons at 90°. To my best knowledge no isotropic events were reported by other authors after Thorne and Andreoli in 1980.

As simultaneous wave measurements either from the ground or space become available, one-to-one correspondence analysis had been reported. Miyoshi et al in 2008 associated an electron precipitation event observed by POES to simultaneous EMIC waves recorded by ground magnetometer. Figure 5.9 is a snapshot of Miyoshi's main findings. The hump of greater than 3 MeV flux on the bottom panel is believed to be evidence of EMIC wave -induced electron precipitation. It is unclear how much of the variation is spatial effort given that POES moves fast at low Earth orbit and both trapped and precipitating electrons at lower energy also see a big hump. Furthermore, the trapped 3 MeV electron flux is not available for comparison to precipitating electrons. The wave amplitude in space was estimated from the ground-based observation. The diffusion coefficient was then estimated with assumptions on the wave properties and cold plasma condition. Miyoshi's conclusion is EMIC waves caused the observed electron and proton precipitation.

Rodger et al in 2015 [42] reported a burst of protons and electrons precipitation observed by POES when Van Allen probe at conjunction observes strong helium band wave at L greater than 5. The precipitating electron flux is estimated to be $1.25 \times 10^4\ cm^{-2}s^{-1}sr^{-1}$ at energy above 140-230 keV. The POES trapped electron flux is not reported. From eyeball estimation of trapped electron flux from Van Allen probes in Figure 4 of Rodger 's paper, the trapped electron flux near the edge of loss cone is at least one order of magnitude higher than estimated precipitating flux and even higher at higher pitch angles. The diffusion coefficient is not given by Rodger. It is unknown how close is the observation to the theory. As

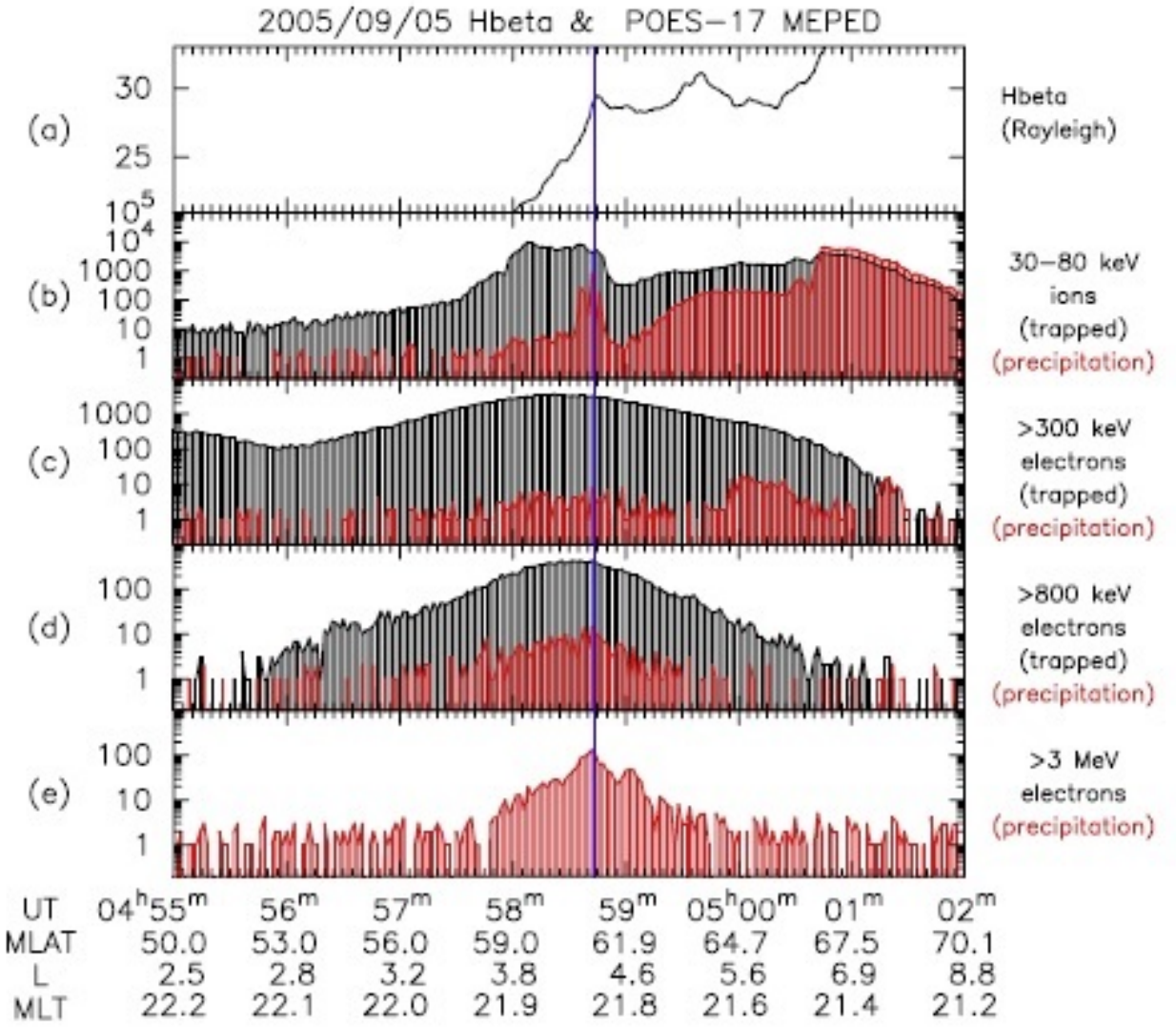

Figure 5.9: snapshot of Figure 3 of Miyoshi et al 2008 [38].(a) Emission profile of Hb and (be) count rates of energetic ions and electrons observed by POES-17 on September 5, 2005 with UT, MLAT, the McIlwain L-value, and magnetic local time (MLT) of the satellite footprint during the period when the satellite was crossing over Athabasca. The vertical blue line indicates the time when the satellite footprint crossed the stable isolated proton aurora. MLAT and L-value are calculated by the IGRF model.

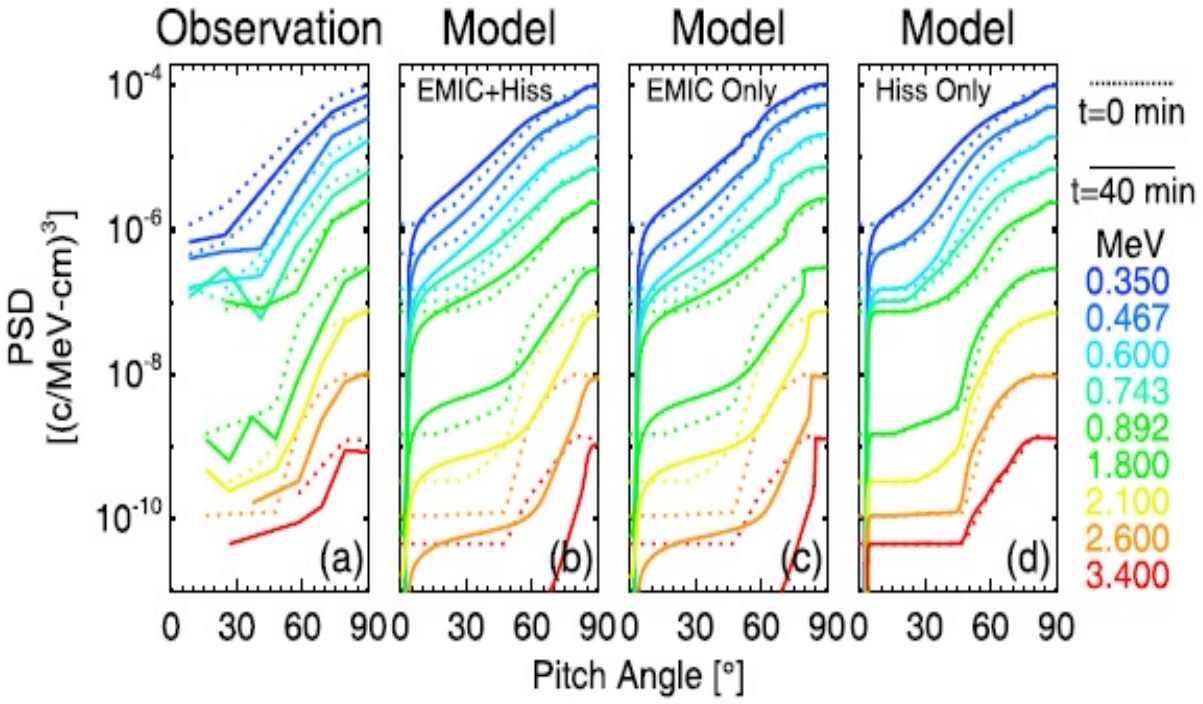

Figure 5.10: Snapshot of Figure 8 of Zhang XJ et al 2016 [56].(a) Observed electron pitch angle distributions from Van Allen Probes at L = 5.77. (b) The evolution of electron distribution after interaction with EMIC and hiss, (c) only EMIC, and (d) only hiss waves for 40 min. Initial distributions are shown in dotted lines; observations or model results at t = 40 min are shown in solid lines.

demonstrated in case 1 study in previous sections, simultaneous observations of EMIC waves and electron precipitation doesn't necessarily imply EMIC wave causes the precipitation.

Contrarily to Rodger's findings, as mentioned in Chapter 1, Usanova and Engebretson reported the absence of electron precipitation at the presence of strong and long lasting EMIC waves. The amount of electrons is too low to be detected by POES. The findings in this thesis agree with Usanova and Engebreson's findings. There is no evidence of significant loss of electrons caused by EMIC waves.

Before drawing conclusion for this chapter, it is worthwhile to investigate greater than 2 MeV electrons. Though EMIC seems to be ineffective at scattering electrons with energy smaller than 2 MeV, it is still possible that EMIC wave is able to precipitate electrons at ultra-relativistic energies. Both Usanova and Engebretson reported the pitch angle distribution of several MeV electrons is more pancake-like at the presence of EMIC wave. Zhang XJ et al in 2016 [56] simulated EMIC wave diffusion for a pancake case by taking advantage of identical orbit and time elapse between the two Van Allen probes. Figure 5.10 is snapshot of Figure 8 in Zhang XJ's paper. The Van Allen probe B and A went through the same point in time lapse of 40 min. The observation from probe B is used as initial condition for the simulation. The simulation agrees with the observations at energy greater than 1.8 MeV and medium pitch angles. It does not reproduce the electron profile at lower energy. These findings agree with one of the findings in this thesis that the discrepancy between measurement and theory inside loss cone decreases at higher energy. This could give a guidance to the direction of theory modifications.

5.4 Conclusions of testing EMIC wave diffusion theory

In summary, three EMIC wave events have been analyzed. The first case shows isotropic distribution which results from process other than EMIC wave scattering. It demonstrates that simultaneous presence of electron precipitation and EMIC waves doesn't guarantee any connection between the two. A large discrepancy between observation and what EMIC wave diffusion theory predicts is found from the second case. If EMIC wave were able to precipitate electrons from several hundred keV to about 2 MeV, the magnitude of diffusion should be significantly smaller than what current theory suggests. In the third case the resonant energy is much higher than the upper limit of electron detector, no conclusion is drawn from that. It is likely that EMIC wave is more effective at higher energies.

Chapter 6

CONCLUSION AND FUTURE WORK

Hiss, EMIC and chorus waves have been the three major waves included in radiation belt electron models and simulations by many space scientists. Two of the three waves , hiss and EMIC waves are tested against the electron loss cone distribution in this thesis. The loss cone electron pitch angle distribution that can be completely explained by hiss diffusion theory is found. Hiss wave is also found to be far insufficient to account for the electron precipitation among 25 out of 38 cases. Only 4 out of the 25 cases see the presence of either chorus or EMIC waves, which suggests loss mechanisms other than the three major waves modes are present. The strong diffusion of electrons predicted by EMIC wave theory has not been found. Current quasi-linear theory of EMIC wave diffusion significantly overestimates the electron precipitation by EMIC waves at energy up to at least 2 MeV. More observations at ultra-relativistic energies are needed to quantitatively evaluate the role of EMIC wave in radiation belt electron loss.

BIBLIOGRAPHY

[1] J. M. Albert. Quasi-linear pitch angle diffusion coefficients: Retaining high harmonics. *Journal of Geophysical Research: Space Physics*, 99(A12):23741–23745, 1994.

[2] J. M. Albert. Analysis of quasi-linear diffusion coefficients. *Journal of Geophysical Research: Space Physics*, 104(A2):2429–2441, 1999.

[3] J. M. Albert. Evaluation of quasi-linear diffusion coefficients for emic waves in a multispecies plasma. *Journal of Geophysical Research: Space Physics*, 108(A6), 2003.

[4] B. J. Anderson, R. E. Erlandson, and L. J. Zanetti. A statistical study of pc 12 magnetic pulsations in the equatorial magnetosphere: 1. equatorial occurrence distributions. *Journal of Geophysical Research: Space Physics*, 97(A3):3075–3088, 1992.

[5] ROGER R. ANDERSON, DONALD A. GURNETT, and DANIEL L. ODEM. Crres plasma wave experiment. *Journal of Spacecraft and Rockets*, 29(4):570–573, Jul 1992.

[6] Hendry A.T. *Experimental evidence and properties of EMIC wave driven electron precipitation (Thesis, Doctor of Philosophy)*. University of Otago, 2018.

[7] L. W. Blum, A. Halford, R. Millan, J. W. Bonnell, J. Goldstein, M. Usanova, M. Engebretson, M. Ohnsted, G. Reeves, H. Singer, M. Clilverd, and X. Li. Observations of coincident emic wave activity and duskside energetic electron precipitation on 1819 january 2013. *Geophysical Research Letters*, 42(14):5727–5735, 2015.

[8] A. W. Breneman, A. Halford, R. Millan, M. McCarthy, J. Fennell, J. Sample, L. Woodger, G. Hospodarsky, J. R. Wygant, C. A. Cattell, J. Goldstein, D. Malaspina, and C. A. Kletzing. Global-scale coherence modulation of radiation-belt electron loss from plasmaspheric hiss. *Nature*, 523:193 EP –, Jun 2015.

[9] Max D. Comess, David M. Smith, Richard S. Selesnick, Robyn M. Millan, and John G. Sample. Duskside relativistic electron precipitation as measured by sampex: A statistical survey. *Journal of Geophysical Research: Space Physics*, 118(8):5050–5058, 2013.

[10] G. Davidson and M. Walt. Loss cone distributions of radiation belt electrons. *Journal of Geophysical Research*, 82(1):48–54, 1977.

[11] R E. Denton, V K. Jordanova, and J Bortnik. Resonance of relativistic electrons with eletromagnetic ion cyclotron waves. *Geophys. Res.Lett*, 2015.

[12] M. J. Engebretson, J. L. Posch, J. R. Wygant, C. A. Kletzing, M. R. Lessard, C.-L. Huang, H. E. Spence, C. W. Smith, H. J. Singer, Y. Omura, R. B. Horne, G. D. Reeves, D. N. Baker, M. Gkioulidou, K. Oksavik, I. R. Mann, T . Raita, and K. Shiokawa. Van allen probes, noaa, goes, and ground observations of an intense emic wave event extending over 12 h in magnetic local time. *Journal of Geophysical Research: Space Physics*, 120(7):5465–5488, 2015.

[13] B.J. Fraser and T.S. Nguyen. Is the plasmapause a preferred source region of electromagnetic ion cyclotron waves in the magnetosphere? *Journal of Atmospheric and Solar-Terrestrial Physics*, 63(11):1225 – 1247, 2001. The Plasmasphere Revisited: A Tribute to Donald Carpenter.

[14] Yuzhu Gao, Fuliang Xiao, Qi Yan, Chang Yang, Si Liu, Yihua He, and Qinghua Zhou. Influence of wave normal angles on hiss-electron interaction in earth's slot region. *Journal of Geophysical Research: Space Physics*, 120(11):9385–9400, 2015. 2015JA021786.

[15] Rachael Hardman, Mark A. Clilverd, Craig J. Rodger, James B. Brundell, Roger Duthie, Robert H. Holzworth, Ian R. Mann, David K. Milling, and Eva Macusova. A case study of electron precipitation fluxes due to plasmaspheric hiss. *Journal of Geophysical Research: Space Physics*, 120(8):6736–6748, 2015. 2015JA021429.

[16] W. L. Imhof, R. R. Anderson, J. B. Reagan, and E. E. Gaines. Coordinated measurements of slot region electron precipitation by plasmaspheric wave bands. *Journal of Geophysical Research: Space Physics*, 87(A6):4418–4426, 1982.

[17] W. L. Imhof, D. L. Chenette, E. E. Gaines, and J. D. Winningham. Characteristics of electrons at the trapping boundary of the radiation belt. *Journal of Geophysical Research: Space Physics*, 102(A1):95–104, 1997.

[18] W. L. Imhof, R. M. Robinson, H. L. Collin, J. R. Wygant, and R. R. Anderson. Simultaneous equatorial measurements of waves and precipitating electrons in the outer radiation belt. *Geophysical Research Letters*, 19(24):2437–2440, 1992.

[19] W. L. Imhof, R. M. Robinson, H. L. Collin, J. R. Wygant, and R. R. Anderson. Simultaneous measurements of waves and precipitating electrons near the equator in the outer radiation belt. *Journal of Geophysical Research: Space Physics*, 99(A2):2415–2427, 1994.

[20] W. L. Imhof, H. D. Voss, J. B. Reagan, D. W. Datlowe, E. E. Gaines, J. Mobilia, and D. S. Evans. Relativistic electron and energetic ion precipitation spikes near the plasmapause. *Journal of Geophysical Research: Space Physics*, 91(A3):3077–3088, 1986.

[21] Juro Ishida, Susumu Kokubun, and Robert L. McPherron. Substorm effects on spectral structures of pc 1 waves at synchronous orbit. *Journal of Geophysical Research: Space Physics*, 92(A1):143–158, 1987.

[22] M. H. Johnson and John Kierein. Combined release and radiation effects satellite (crres): Spacecraft and mission. *Journal of Spacecraft and Rockets*, 29(4):556–563, Jul 1992.

[23] S. Kasahara, Y. Miyoshi, S. Yokota, T. Mitani, Y. Kasahara, S. Matsuda, A. Kumamoto, A. Matsuoka, Y. Kazama, H. U. Frey, V. Angelopoulos, S. Kurita, K. Keika, K. Seki, and I. Shinohara. Pulsating aurora from electron scattering by chorus waves. *Nature*, 554:337 EP –, Feb 2018.

[24] C. F. Kennel and H. E. Petschek. Limit on stably trapped particle fluxes. *Journal of Geophysical Research*, 71(1):1–28, 1966.

[25] G. V. Khazanov and K. V. Gamayunov. Effect of emic wave normal angle distribution on relativistic electron scattering in outer rb. *NASA Marshall Space Flight Center; Huntsville, AL, United States*, 2007.

[26] W. Li, B. Ni, R. M. Thorne, J. Bortnik, Y. Nishimura, J. C. Green, C. A. Kletzing, W. S. Kurth, G. B. Hospodarsky, H. E. Spence, G. D. Reeves, J. B. Blake, J. F. Fennell, S. G. Claudepierre, and X. Gu. Quantifying hiss-driven energetic electron precipitation: A detailed conjunction event analysis. *Geophysical Research Letters*, 41(4):1085–1092, 2014. 2013GL059132.

[27] Zan Li, Robyn M. Millan, Mary K. Hudson, Leslie A. Woodger, David M. Smith, Yue Chen, Reiner Friedel, Juan V. Rodriguez, Mark J. Engebretson, Jerry Goldstein, Joseph F. Fennell, and Harlan E. Spence. Investigation of emic wave scattering as the cause for the barrel 17 january 2013 relativistic electron precipitation event: A quantitative comparison of simulation with observations. *Geophysical Research Letters*, 41(24):8722–8729, 2014.

[28] L. R. Lyons, R. M. Thorne, and C. F. Kennel. Electron pitch-angle diffusion driven by oblique whistler-mode turbulence. *Journal of Plasma Physics*, 6(3):589606, 1971.

[29] Lawrence R. Lyons. Pitch angle and energy diffusion coefficients from resonant interactions with ioncyclotron and whistler waves. *Journal of Plasma Physics*, 12(3):417432, 1974.

[30] Lawrence R. Lyons and Richard Mansergh Thorne. Parasitic pitch angle diffusion of radiation belt particles by ion cyclotron waves. *Journal of Geophysical Research*, 77(28):5608–5616, 1972.

[31] Lawrence R. Lyons and Richard Mansergh Thorne. Equilibrium structure of radiation belt electrons. *Journal of Geophysical Research*, 78(13):2142–2149, 1973.

[32] Lawrence R. Lyons, Richard Mansergh Thorne, and Charles F. Kennel. Pitch-angle diffusion of radiation belt electrons within the plasmasphere. *Journal of Geophysical Research*, 77(19):3455–3474, 1972.

[33] Spasojevic . M. Statistics of auroral hiss and relationship to auroral boundaries and upward current regions. *Journal of Geophysical Research: Space Physics*, 2016.

[34] Nigel P. Meredith, Richard B. Horne, Sarah A. Glauert, and Rodger R. Anderson. Slot region electron loss timescales due to plasmaspheric hiss and lightning-generated whistlers. *Journal of Geophysical Research: Space Physics*, 2007.

[35] Nigel P. Meredith, Richard B. Horne, Sarah A. Glauert, Richard M. Thorne, Danny Summers, Jay M. Albert, and Roger R. Anderson. Energetic outer zone electron loss timescales during low geomagnetic activity. *Journal of Geophysical Research: Space Physics*, 111(A5):n/a–n/a, 2006. A05212.

[36] Nigel P. Meredith, Richard M. Thorne, Richard B. Horne, Danny Summers, Brian J. Fraser, and Roger R. Anderson. Statistical analysis of relativistic electron energies for cyclotron resonance with emic waves observed on crres. *Journal of Geophysical Research: Space Physics*, 108(A6), 2003.

[37] R. M. Millan, R. P. Lin, D. M. Smith, K. R. Lorentzen, and M. P. McCarthy. X-ray observations of mev electron precipitation with a balloon-borne germanium spectrometer. *Geophysical Research Letters*, 29(24):47–1–47–4, 2002.

[38] Y. Miyoshi, K. Sakaguchi, K. Shiokawa, D. Evans, J. Albert, M. Connors, and V. Jordanova. Precipitation of radiation belt electrons by emic waves, observed from ground and space. *Geophysical Research Letters*, 35(23), 2008.

[39] Yoshiharu Omura and Qinghua Zhao. Relativistic electron microbursts due to nonlinear pitch angle scattering by emic triggered emissions. *Journal of Geophysical Research: Space Physics*, 118(8):5008–5020, 2013.

[40] Carl A. Reber. The upper atmosphere research satellite (uars). *Geophysical Research Letters*, 20(12):1215–1218, 1993.

[41] Charles S. Roberts. Pitch-angle diffusion of electrons in the magnetosphere. *Reviews of Geophysics*, 7(1-2):305–337, 1969.

[42] Craig J. Rodger, Aaron T. Hendry, Mark A. Clilverd, Craig A. Kletzing, James B. Brundell, and Geoffrey D. Reeves. High-resolution in situ observations of electron precipitation-causing emic waves. *Geophysical Research Letters*, 42(22):9633–9641, 2015.

[43] A. A. Saikin, J.-C. Zhang, R. C. Allen, C. W. Smith, L. M. Kistler, H. E. Spence, R. B. Torbert, C. A. Kletzing, and V. K. Jordanova. The occurrence and wave properties of h+-, he+-, and o+-band emic waves observed by the van allen probes. *Journal of Geophysical Research: Space Physics*, 120(9):7477–7492, 2015.

[44] H. J. SINGER, W. P. SULLIVAN, PETER ANDERSON, F. MOZER, P. HARVEY, J. WYGANT, and WILLIAM MCNEIL. Fluxgate magnetometer instrument on the crres. *Journal of Spacecraft and Rockets*, 29(4):599–601, Jul 1992.

[45] David M. Smith, Eric P. Casavant, Max D. Comess, Xinqing Liang, Gregory S. Bowers, Richard S. Selesnick, Lasse B. N. Clausen, Robyn M. Millan, and John G. Sample. The causes of the hardest electron precipitation events seen with sampex. *Journal of Geophysical Research: Space Physics*, 121(9):8600–8613, 2016.

[46] Danny Summers and Richard M. Thorne. Relativistic electron pitch-angle scattering by electromagnetic ion cyclotron waves during geomagnetic storms. *Journal of Geophysical Research: Space Physics*, 108(A4), 2003.

[47] R. M. Thorne and C. F. Kennel. Relativistic electron precipitation during magnetic storm main phase. *Journal of Geophysical Research*, 76(19):4446–4453, 1971.

[48] R. M. Thorne, W. Li, B. Ni, Q. Ma, J. Bortnik, D. N. Baker, H. E. Spence, G. D. Reeves, M. G. Henderson, C. A. Kletzing, W. S. Kurth, G. B. Hospodarsky, D. Turner, and V. Angelopoulos. Evolution and slow decay of an unusual narrow ring of relativistic electrons near l 3.2 following the september 2012 magnetic storm. *Geophysical Research Letters*, 40(14):3507–3511, 2013.

[49] Andreoli L.J. Thorne R.M. *Exploration of the Polar Upper Atmosphere. NATO Advanced Study Institutes Series (Series C Mathematical and Physical Sciences)*. Springer, Dordrecht, 1980.

[50] M. E. Usanova, A. Drozdov, K. Orlova, I. R. Mann, Y. Shprits, M. T. Robertson, D. L. Turner, D. K. Milling, A. Kale, D. N. Baker, S. A. Thaller, G. D. Reeves, H. E. Spence, C. Kletzing, and J. Wygant. Effect of emic waves on relativistic and ultrarelativistic electron populations: Ground-based and van allen probes observations. *Geophysical Research Letters*, 41(5):1375–1381, 2014.

[51] A. L. Vampola. Electron pitch angle scattering in the outer zone during magnetically disturbed times. *Journal of Geophysical Research*, 76(19):4685–4688, 1971.

[52] A. L. VAMPOLA, J. V. OSBORN, and B. M. JOHNSON. Crres magnetic electron spectrometer afgl-701-5a (mea). *Journal of Spacecraft and Rockets*, 29(4):592–595, Jul 1992.

[53] JAMES A. VAN ALLEN and LOUIS A. FRANK. Radiation around the earth to a radial distance of 107,400 km. *Nature*, 183:430 EP –, Feb 1959.

[54] J. D. Winningham, J. R. Sharber, R. A. Frahm, J. L. Burch, N. Eaker, R. K. Black, V. A. Blevins, J. P. Andrews, J. Rudzki, M. J. Sablik, D. L. Chenette, D. W. Datlowe, E. E. Gaines, W. I. Imhof, R. W. Nightingale, J. B. Reagan, R. M. Robinson, T. L. Schumaker, E. G. Shelley, R. R. Vondrak, H. D. Voss, P. F. Bythrow, B. J. Anderson, T. A. Potemra, L. J. Zanetti, D. B. Holland, M. H. Rees, D. Lummerzheim, G. C. Reid, R. G. Roble, C. R. Clauer, and P. M. Banks. The uars particle environment monitor. *Journal of Geophysical Research: Atmospheres*, 98(D6):10649–10666, 1993.

[55] Jichun Zhang, Alexa J. Halford, Anthony A. Saikin, Chia-Lin Huang, Harlan E. Spence, Brian A. Larsen, Geoffrey D. Reeves, Robyn M. Millan, Charles W. Smith, Roy B. Torbert, William S. Kurth, Craig A. Kletzing, J. Bernard Blake, Joseph F. Fennel, and Daniel N. Baker. Emic waves and associated relativistic electron precipitation on 2526 january 2013. *Journal of Geophysical Research: Space Physics*, 121(11):11,086–11,100, 2016.

[56] X.-J. Zhang, W. Li, Q. Ma, R. M. Thorne, V. Angelopoulos, J. Bortnik, L. Chen, C. A. Kletzing, W. S. Kurth, G. B. Hospodarsky, D. N. Baker, G. D. Reeves, H. E. Spence, J. B. Blake, and J. F. Fennell. Direct evidence for emic wave scattering of relativistic electrons in space. *Journal of Geophysical Research: Space Physics*, 121(7):6620–6631, 2016.

[57] X.-J. Zhang, W. Li, R. M. Thorne, V. Angelopoulos, J. Bortnik, C. A. Kletzing, W. S. Kurth, and G. B. Hospodarsky. Statistical distribution of emic wave spectra: Observations from van allen probes. *Geophysical Research Letters*, 43(24):12,348–12,355, 2016.

Appendix A

A.1 Derivation of $N(\omega)$ for hiss diffusion coefficient

In a volume V, the total magnetic energy can be expressed in terms of either on frequency ω or wave vector $\mathbf{k}$ domain

$$V\int_0^\infty B^2(\omega)d\omega = \frac{1}{(2\pi)^3}\int |\mathbf{B_k}|^2\, d^3\mathbf{k} = \frac{1}{(2\pi)^2}\int_0^\infty k_\perp dk_\perp \int_{-\infty}^\infty dk_\parallel\, |\mathbf{B_k}|^2 \tag{A.1}$$

By plugging 3.13 and transforming from $(k_\perp, k_\parallel)$ to $(\omega, X = \tan\theta)$ domain, the relationship is rewritten as

$$\int_0^\infty B^2(\omega)d\omega = \frac{2}{(2\pi)^2}\int_0^\infty B^2(\omega)\frac{\int_0^\infty g(X)k_\perp J(\frac{k_\parallel}{\omega}, \frac{k_\perp}{X})dX}{N(\omega)}d\omega \tag{A.2}$$

Thus

$$N(\omega) = \frac{2}{(2\pi)^2}\int_0^\infty g(X)k_\perp J(\frac{k_\parallel}{\omega}, \frac{k_\perp}{X})dX \tag{A.3}$$

Jacobian is given by

$$J(\frac{k_\parallel}{\omega}, \frac{k_\perp}{X}) = \begin{vmatrix} \frac{\partial k_\parallel}{\partial \omega} & \frac{\partial k_\perp}{\partial \omega} \\ \frac{\partial k_\parallel}{\partial X} & \frac{\partial k_\perp}{\partial X} \end{vmatrix} \tag{A.4}$$

With the help of simplified cold plasma dispersion relation for whistler wave $\frac{c^2k^2}{\omega^2} = \frac{\omega_{pe}^2}{\omega\Omega_e cos\theta}$, The four terms in the determinant collapses to two terms and Jacobian is rewritten as

$$J(\frac{k_\parallel}{\omega}, \frac{k_\perp}{X}) = (\frac{\omega_{pe}}{c})^3\frac{1}{2k_\perp\Omega_e}(\frac{\omega}{\Omega_e})^{\frac{1}{2}}X(1+X^2)^{-\frac{3}{4}} \tag{A.5}$$

Finally, the normalization factor is given by

$$N(\omega) = \frac{1}{(2\pi)^2}\frac{\omega^{\frac{1}{2}}}{\Omega_e^{\frac{3}{2}}}(\frac{\omega_{pe}}{c})^3\int_{X_{min}}^{X_{max}} Xg(X)(1+X^2)^{-\frac{3}{4}}dX = \frac{1}{(2\pi)^2}\frac{\omega^{\frac{1}{2}}}{\Omega_e^{\frac{3}{2}}}(\frac{\omega_{pe}}{c})^3 I \tag{A.6}$$

A.2 Derivation of $N(Y)$ for EMIC diffusion coefficient

The Jacobian from EMIC wave dispersion relation is

$$J(\frac{k_{\parallel}}{\omega}, \frac{k_{\perp}}{X}) = \left| \frac{\omega_{pe}^2 M^2 X Y^2}{2\Omega_e c^2 \Psi^2} \left(\frac{2MY\omega_{pe}^2}{c^2 k_{\parallel}} - \frac{k_{\parallel}}{M} \frac{\partial \Psi}{\partial Y} \right) \right| \tag{A.7}$$

Thus $N(Y)$ is given by

$$N(Y) = \frac{\omega_{pe}^2 M^2 Y^2}{(2\pi)^2 \Omega_e c^2} \int_{X_{min}}^{X_{max}} dX g(X) \frac{X}{\Psi^2} \left| \left(\frac{2MY\omega_{pe}^2}{c^2 k_{\parallel}} - \frac{k_{\parallel}}{M} \frac{\partial \Psi}{\partial Y} \right) \right| \tag{A.8}$$

A.3 Source term estimation using observations inside loss cone

At low Earth orbit (UARS location) each of the three UARS electron telescopes inside loss cone measures differential electron flux J_i, $i = 1, 2, 3$, the unit of J_i is $s^{-1}cm^{-2}sr^{-1}keV^{-1}$. Assume $d\Omega = \sin\theta d\theta d\phi$ is the solid angle element, where θ is the angle from local magnetic field B and ϕ is azimuthal angle around B. The total integral electron flux inside loss cone is then determined by

$$J_{total} = \sum_i \int_{\Omega_i} J_i d\Omega = \sum_i \int_{\Omega_i} J_i \sin\theta d\theta d\phi = 2\pi \sum_i \int_{\Omega_i} J_i \sin\theta d\theta \tag{A.9}$$

where flux azimuthal symmetry is assumed, the integral range Ω_i for each telescope is a ring-shape patch that is created by spinning telescope around local magnetic field and determined by the field of view of the telescope, the angle between center of the telescope and local magnetic field B, and adjusted for overlaps between two adjacent telescopes and the boundary of loss cone at UARS. The unit of J_{total} is $s^{-1}cm^{-2}keV^{-1}$. J_{total} is also given by

$$J_{total} = \int_{losscone} J d\Omega \tag{A.10}$$

where the integral is over entire loss cone and the differential flux J is related to distribution function by

$$J = P^2 f_{\mathbf{P}}(\mathbf{P}) = \frac{P^2}{m^3} f_v(\alpha_0, v) \tag{A.11}$$

where P and m are momentum and mass of electrons, $f_v(\alpha_0, v)$ is the loss cone solution given by 3.3 and copied here with subscript v omitted

$$f(\alpha_0, v) = \frac{S(v)}{D^*} h(\alpha_0) = \frac{S(v)}{D^*} \frac{\sqrt{D^* T_E}}{\alpha_c} \frac{I_0(\alpha_0/\sqrt{D^* T_E})}{I_1(\alpha_c/\sqrt{D^* T_E})} \tag{A.12}$$

Source term $S(v)$ is determined by equating the theoretical flux from distribution function and measurement from UARS.

A.4 Some notes on diffusion coefficients code implementation and testing

The diffusion coefficients formulas for both hiss and EMIC waves in Chapter 3 are implemented in MATLAB. Contact me if you are interested in using or testing my code.

In Lyons et al 1972 [32], Gaussian models for hiss wave frequency and normal angle distribution were adopted. I first implemented Lyons' 72 diffusion coefficient formulas and reproduced Figure 4 of Lyons et al 1972[32]. This figure shows how cyclotron and Landau resonance diffusion coefficients varying with equatorial pitch angle with arbitrary unit. In order to have a sense of the magnitude of diffusion coefficients, the outputs of my code were compared to Figure 1 of Albert 1994 [1]. Albert's plot is based on the same parameters used by Lyons et al 1972 except with wave amplitude specified. My code reproduces Albert's plot. The code outputs were also compared to results from several other authors (e.g. Gao et al 2015 [14]). The agreements were found. Once the Gaussian diffusion coefficient code was tested, I then implemented the more general version of the diffusion coefficient formula 3.20 and tested against the Gaussian code. The two sets of code give exactly the same diffusion coefficients with identical Gaussian wave inputs.

EMIC wave code has the same structure as hiss wave code except the implementation of dispersion relationship. The dispersion relationship of EMIC wave is far more complicated than hiss wave, which makes the code more complicated and computationally expensive. The dispersion relationship part was tested heavily against results from Albert 2003[3]. Figure 1 and 2 in Albert 2003[3] were reproduced and similar plots were obtained when the parameters were tweaked. The diffusion coefficients were also compared to Summers 2003[46]. My

diffusion coefficients are one order of magnitude lower than Summers'. That is because the bounce averaged diffusion coefficient is one order of magnitude lower than local equatorial values as mentioned in Summers 2003.

VITA

As the first college student in my direct family since my great great-grand father and the first graduate student from my extended family since early 20th century, I thank everyone in both my immediate and extended family for great support for so many years. I also thank the help from friends I made in elementary school, middle school, high school, college and now, both in China and in United States.